Heliyon 9 (2023) e22051

Contents lists available at ScienceDirect

Heliyon

journal homepage: www.cell.com/heliyon

Effect of herbal extracts and Saroglitazar on high-fat diet-induced obesity, insulin resistance, dyslipidemia, and hepatic lipidome in C57BL/6J mice

Deepika Kumari, Jyoti Gautam, Vipin Sharma, Sonu Kumar Gupta, Soumalya Sarkar, Pradipta Jana, Vikas Singhal, Prabhakar Babele, Parul Kamboj, Sneh Bajpai, Ruchi Tandon [1], Yashwant Kumar [*], Madhu Dikshit [1,2,*]

Non-communicable Disease Centre, Translational Health Science and Technology Institute (THSTI), NCR Biotech Science Cluster, 3rd Milestone, Faridabad, 121001, Haryana, India

ARTICLE INFO

Keywords:
DIO mouse model
Insulin resistance
Inflammation
Fibrosis
Liver lipidome
Saroglitazar
Tinospora cordifolia and *Piper longum*

ABSTRACT

We evaluated the effects of select herbal extracts (*Tinospora cordifolia* [TC], *Tinospora cordifolia* with *Piper longum* [TC + PL], *Withania somnifera* [WS], *Glycyrrhiza glabra* [GG], AYUSH–64 [AY-64], and Saroglitazar [S]) on various parameters in a diet-induced obesity mouse model. After 12 weeks of oral administration of the herbal extracts in high-fat diet (HFD)-fed C57BL/6J mice, we analyzed plasma biochemical parameters, insulin resistance (IR), liver histology, and the expression of inflammatory and fibrosis markers, along with hepatic lipidome. We also used a 3D hepatic spheroid model to assess their impact on profibrotic gene expression. Among the extracts, TC + PL showed a significant reduction in IR, liver weight, *TNF-α*, *IL4*, *IL10* expression, and hepatic lipid levels (saturated triglycerides, ceramides, lysophosphocholines, acylcarnitines, diglycerides, and phosphatidylinositol levels). Saroglitazar reversed changes in body weight, IR, plasma triglycerides, glucose, insulin, and various hepatic lipid species (fatty acids, phospholipids, glycerophospholipids, sphingolipids, and triglycerides). With the exception of GG, Saroglitazar, and other extracts protected against palmitic acid-induced fibrosis marker gene expression in the 3D spheroids. TC + PL and Saroglitazar also effectively prevented HFD-induced insulin resistance, inflammation, and specific harmful lipid species in the liver.

1. Introduction

Botanicals described in Ayurvedic texts and traditional medicine systems offer numerous health benefits and have been used for centuries to safeguard both humans and animals from infectious and non-communicable diseases. Throughout the COVID-19 pandemic, the AYUSH ministry in India recommended several commonly used herbal medicines to prevent SARS-CoV-2 infection and its associated complications. In our study, we assessed the protective effects of herbal extracts against SARS-CoV-2 infection in cell-based and animal models, as well as their potential for immunomodulation. These evaluations were also conducted in our lab as well as

* Central Drug Research Institute, Sitapur Rd, Sector 10, Jankipuram Extension, Lucknow, Uttar Pradesh, 226031, India.
E-mail addresses: y.kumar@thsti.res.in (Y. Kumar), drmadhudikshit@gmail.com, madhu.dikshit@cdri.res.in (M. Dikshit).
[1] Current address.
[2] Lead Contact.

https://doi.org/10.1016/j.heliyon.2023.e22051
Received 11 December 2022; Received in revised form 2 November 2023; Accepted 2 November 2023
Available online 4 November 2023

Abbreviations

AcCar	Acylcarnitine
AUC	Area under the curve
AY-64	AYUSH- 64
BMI	Body mass index
Cer	Ceramide
CMC	Carboxymethylcellulose
DAG	diacylglycerol
GG	*Glycyrrhiza glabra*
H&E	Hematoxylin and eosin
HFD	High-fat diet
HFHF	High-fructose high-fat
HOMA	The homeostasis model assessment
HPLC	high-performance liquid chromatography
IP	Intraperitoneal
IPGTT	Intraperitoneal glucose tolerance test
IR	Insulin resistance
LPC	Lysophosphatidylcholine
MT	Masson's trichrome
NAFLD	Nonalcoholic fatty liver disease
NASH	Nonalcoholic steatohepatitis
PI	Phosphatidylinositol
PL	*Piper longum*
QUICKI	Quantitative insulin sensitivity check index
S	Saroglitazar
T2DM	Type 2 diabetes mellitus
TC	*Tinospora cordifolia*
TG	Triglyceride
UPLC	Ultra-performance liquid chromatography
V	Vehicle
WS	*Withania somnifera*

by other researchers. Furthermore, it was observed that individuals with Type 2 diabetes (T2DM) were particularly susceptible to SARS-CoV-2 infection and experienced more severe COVID-19-related complications during the pandemic.

High consumption of both high-fat and high-sugar diets, coupled with a sedentary lifestyle, increases the risk of obesity, insulin resistance (IR), T2DM, cardiovascular issues, and non-alcoholic fatty liver disease (NAFLD) [1–3]. Oxidative stress, inflammatory cytokines, mitochondrial dysfunction, and abnormal lipid metabolism play crucial roles in the progression of diabetes and hepatic steatosis [4–7]. Improvements in obesity, IR, and hyperglycemia can reverse both T2DM and fatty liver conditions. Several herbal extracts possess antioxidant, anti-obesity, anti-inflammatory, and antidiabetic properties, enhancing insulin sensitivity and reducing hyperglycemia [8–11]. Herbal formulations, due to their diverse bioactive constituents, demonstrate multi-targeting potential [8–11].

The herbal extracts utilized in this study have well-documented anti-inflammatory, antidiabetic, and hepatoprotective properties. A polyherbal extract comprising *Tinospora cordifolia, Andrographis paniculata, and Solanum nigrum* exhibited hepatoprotective effects in Swiss albino mice [12]. Additionally, treatment with TC provided protection against IR, oxidative stress, obesity, and various diabetic complications in rats [12–15]. *Piper longum* and its constituents, including piperine, also demonstrated moderate hepatoprotective effects and protection against liver fibrosis [16,17].

Withaferin A (WF-A), a bioactive compound from Withania somnifera (WS), exhibited anti-obesity effects and reversed hepatic steatosis in mice [18,]. WF-A also provided protection against nonalcoholic steatohepatitis (NASH) induced by methionine-choline-deficient (MCD) and high-fat diets in mice [19]. WS improved liver function, reduced oxidative stress, enhanced insulin sensitivity, and demonstrated anti-hyperglycemic properties in rat models of hepatic encephalopathy and T2DM [20,21].

Supplementing GG extract with a low-calorie diet in obese individuals reduced fat mass and IR [22]. GG and its components have shown cholesterol-lowering and anti-obesity effects in rodent models [23]. Moreover, GG supplementation improved glucose tolerance, decreased the expression of inflammatory markers (TNF-α and IL-6), reduced liver triglyceride levels, alleviated fatty liver conditions, and exhibited hepatoprotective and anti-hyperglycemic properties in multiple studies [24–27]. Additionally, glycyrrhizic acid prevented cytotoxicity induced by aflatoxin in hepatoma cells [28].

AYUSH-64, a mixture of multiple herbs (Saptaparna; *Alstonia scholaris*, Kutaki; *Picrorhiza kurrao,* Chiraita; *Swertia chirayita*, Lata Karanj; *Caesalpinia cristata*) with anti-inflammatory, immunomodulatory, antioxidant, hypolipidemic [29–32] and antiviral properties [33], controlled COVID-19 symptoms and has been studied for anti-obesity, anti-diabetic, and hypolipidemic effects [34–36].

In this study, we assessed herbal extracts impact on C57BL/6J mice fed HFD, a common model for obesity, IR, dyslipidemia,

NAFLD, and T2DM [37–39]. These mice develop weight gain, hyperglycemia, IR, hyperinsulinemia, and glucose intolerance similar to human metabolic disorders [38].

The liver plays a pivotal role in lipid metabolism and contributes to the regulation of circulating lipid levels [40,41]. In this study, we utilized the DIO mouse model to assess the effects of herbal extracts and Saroglitazar on HFD-induced IR. Furthermore, we investigated how these test substances influenced the lipid species associated with IR. As previously discussed, numerous studies have demonstrated the anti-inflammatory, anti-diabetic, and hepatoprotective properties of the majority of the herbal extracts employed [12–15,18,42,22–27]. Following HFD feeding, we conducted a hepatic lipidome analysis and examined the impact of select herbal extracts. Notably, the TC + PL combination successfully restored toxic lipid levels to normal. Saroglitazar, a dual PPAR α/γ agonist used in India to treat diabetic dyslipidemia and hypertriglyceridemia with T2DM, has also demonstrated benefits in NAFLD/NASH, as supported by clinical trials [43–45]. Our recent findings showed that Saroglitazar protected against high-fat, high-fructose (HFHF) diet-induced obesity, insulin resistance, and steatosis in mice [46]. In our study, Saroglitazar was administered at a dose of 3 mg/kg body weight once daily to HFD-fed mice, while herbal extracts were given twice daily at the human equivalent dose of 110 mg/kg body weight. In this study, we employed the LC-MS/MS technique to conduct a hepatic lipidome analysis after HFD feeding and scrutinized their modification by specific herbal extracts. Among the toxic lipid species identified following HFD administration, the TC + PL combination successfully normalized these levels. To further confirm the anti-fibrotic potential of the test substances, we utilized 3D spheroids of hepatocytes and stellate cells, providing a complex model that mimics the human liver cellular interactions, viability, and metabolic activity [47,48].

The present study demonstrates that with the exception of GG, all tested herbal extracts (TC, WS, AY-64, and TC + PL) and Saroglitazar demonstrated protection against palmitate-induced disruptions in the in vitro 3D spheroid model. The herbal extracts showed no adverse effects on the parameters investigated, and the TC + PL combination provided protection against HFD-induced IR, inflammation, and modulation of toxic lipid species.

2. Material and methods

2.1. Plant material and extraction

All the herbal extracts were supplied by the National Medicinal Plants Board, established by the Government of India from well-authenticated samples, as is reported in the previously published reports from this lab [49–55]. Root water extracts of WS and GG, stem water extract of TC, and AY-64 constituents, including rhizome aqueous extracts of *Picrorhiza kurroa*, stem bark aqueous extracts of *Alstonia scholaris*, whole plant aqueous extracts of *Swertia chirayita*, and seed powder extracts of *Cesalpinia cristata*, were prepared under Good Manufacturing Practice conditions.

Briefly, the authenticated crude plant material was ground into a fine powder and passed through a 30-mesh sieve. A decoction of the plant material was then prepared by dissolving it in a 1:10 ratio of solvent (plant material: demineralized water) at a temperature of 55–60 °C for 3 h and filtered through a muslin cloth. The filtrate underwent a distillation process at 55–60 °C under reduced pressure. Subsequently, the extracts were further processed through wiped film evaporation at 80 ± 5 °C, followed by either spray drying or freeze drying, and stored in airtight containers in a cool, dry place. The respective yields (w/w) of the extracts were 10:1, 5–7:1, 10:1, and 15:1 for PL, GG, TC, and WS, respectively. TC and PL were used in a 1:1 ratio in combination experiments. The composition of the aqueous extract was analyzed using high-performance liquid chromatography (HPLC) according to standard protocols [56].

2.2. Animals

Male 8-12-week-old C57BL/6J (20–25 g) mice were procured from the Small Animal Facility (SAF) of the Translational Health Science and Technology Institute (THSTI). Mice were acclimatized at 25 ± 2 °C with a relative humidity of 60 ± 10 % in a pathogen-free environment and, housed under standard laboratory conditions of 12 h light and dark cycle with food and water *ad libitum*. All the animal experiments and the procedures used in study were in accordance with Institutional Animal Ethics Committee (IAEC) of THSTI (protocol approval no. IAEC/THSTI/105, protocol approval date; June 22, 2020).

2.3. Experimental study design and interventions

After a 1-week acclimatization period, the mice were divided into two groups: the first group (n = 6) was fed a normal chow diet (with 11 % fat, 24 % protein, and 65 % carbohydrates, catalog no. 1324 P, Altromin International, Germany), while the remaining mice (n = 42) were provided with a high-fat diet (HFD) (with 60 % fat, 20 % protein, and 20 % carbohydrates, catalog no. D12492, Research Diet Inc., USA). After 4 weeks, measurements of plasma triglycerides (TG), fasting blood glucose levels (FBG), and body weights were taken, and the animals were redistributed into eight groups, each containing 6 mice. Pharmacological interventions commenced 6 weeks after starting the HFD and continued for 18 weeks. The eight groups, each consisting of 6 mice per group, received the following diets and were denoted as normal chow diet (Control), HFD and vehicle (HFD), HFD and Saroglitazar (Zydus Cadila Healthcare Ltd.) (HFD + S, 3 mg/kg orally once daily), HFD and Guduchi (*Tinospora cordifolia*) (HFD + TC, 110 mg/kg orally twice daily), HFD, Guduchi (*Tinospora cordifolia*), and Pippali (*Piper longum*) (HFD + TC + PL, Guduchi 110 mg/kg, 25 (pipli, was given twice (25+25=50)), HFD and Ashwagandha (*Withania somnifera*) (HFD + WS, 110 mg/kg orally twice daily), HFD and Yashtimadhu (*Glycyrrhiza glabra*) (HFD + GG, 110 mg/kg orally twice daily), HFD and AYUSH-64 (HFD + AY-64, 110 mg/kg orally twice daily). Carboxymethylcellulose (CMC) at a concentration of 0.5 %, serving as a vehicle (V), was administered orally to the control (chow diet

group) and HFD-treated groups. In contrast, all the extracts were administered twice a day via the oral route.

Body weights of all the mice were recorded weekly, and FBG and intraperitoneal glucose tolerance tests (IPGTT) were performed after 4 and 18 weeks using a glucometer (Accu-Chek Active, Roche). Body weight and tail/body length were measured, and blood was collected by cardiac puncture after the mice were anesthetized with ketamine (90 mg/kg) and xylazine (10 mg/kg) via intraperitoneal injection after 18 weeks. Liver tissues were collected after sacrificing the mice by cervical dislocation, washed with chilled PBS to remove adherent blood, and the weights were recorded. Both plasma and liver tissue samples were stored in a −80 °C freezer until further analysis.

Systemic insulin sensitivity was assessed through intraperitoneal glucose tolerance test (IPGTT) after a 6-h fasting period, the mice were weighed, and a 20 % glucose solution (2 g of D-glucose/kg body weight) was administered via intraperitoneal (IP) injection to conduct the IPGTT. Blood glucose levels were measured at 0, 15, 30, 60, and 120-min intervals following glucose administration using a glucometer (Accu-Chek Active, Roche), and the area under the curve (AUC) was calculated as previously described [46].

2.4. BMI, QUICKI, and HOMA

The BMI (body mass index) was calculated as the ratio of body weight to square surface area (g/cm2). HOMA-IR (the homeostasis model assessment of insulin resistance) was calculated using the formula: fasting insulin (μIU/mL) × fasting glucose (mg/dL)/405. HOMA-B (the homeostasis model assessment of β-cell function) was evaluated with the formula: 20 × fasting insulin (μIU/mL)/fasting glucose (mmol/mL) − 3.5. QUICKI (quantitative insulin sensitivity check index) was calculated as previously described (1/log fasting insulin (mU/L) + log fasting glucose (mg/dL)) using fasting glucose and insulin values [57].

2.5. Biochemical analyses

Blood plasma was collected following the methods previously outlined [46]. Plasma levels of triglycerides (TG) and total cholesterol (TC) were determined using commercial kits: TRIGS kit (catalogue No. TR1697) and CHOL kit (catalogue No.CH201) from Randox, Crumlin, Co. Antrim, UK. The measurements were conducted in accordance with the manufacturer's instructions. For the assessment of hepatic TG, 50 mg of liver tissue was weighed and homogenized in a 5 % NP-40 buffer. The samples were subjected to heating at 80–100 °C for 2–3 min, followed by cooling on ice, with the process being repeated three times. Subsequently, the samples were centrifuged at 13000×*g* for 10 min, and the levels of TG were measured in the supernatants using the Randox TRIGS kits (catalogue No. TR1697). Insulin concentrations in the plasma samples were determined using commercial kits from Crystal Chem, specifically the Mouse Insulin ELISA kit (catalogue No. 90080) based in Elk Grove Village, IL, USA.

2.6. Liver histology analysis

Hematoxylin and eosin (H&E), Masson's trichrome (MT), and Oil Red O (ORO) staining of liver tissue were conducted following established protocols. Histological assessments, imaging, and scoring were carried out at the National Liver Disease Biobank, Institute of Liver and Biliary Sciences (ILBS), New Delhi, India. The total NASH score was determined by adding up the individual scores for the degree of hepatocellular steatosis, ballooning, inflammation, and fibrosis severity [46].

2.7. RNA isolation, cDNA synthesis, and gene expression analysis using real time PCR

Total RNA was extracted from mouse liver tissues using TRI Reagent (Sigma-Aldrich, T9424). RNA quality and concentration were determined with a NanoDrop spectrophotometer (Thermo Scientific, USA). DNase-treated RNA (2 μg) was reverse-transcribed into single-strand cDNA using oligo dT, dNTPs, and RevertAid Reverse Transcriptase (Thermo Fisher Scientific, Catalogue number: EP0441). Quantitative RT-PCR was conducted to assess gene expression with the QuantStudio 6 Real-Time PCR System (Applied Biosystems, USA), following the method described in our previous study [46]. The primer sequences for each target gene are provided in Table S1. Target gene expression was determined using the ΔΔCt method and normalized to 18S rRNA as the reference gene [46].

3. Hepatic lipidome analysis

3.1. Lipid extraction

Hepatic tissue samples (20 mg) were used for lipid extraction and analysis using a previously established procedure [46,58]. Methanol (0.3 mL) was added to all the samples, followed by thorough vortexing for 30 s. Subsequently, 1.25 mL of methyl-*tert*-butyl ether (MTBE) was added, and the mixture was incubated for 1 h on a shaker at room temperature. To induce phase separation, 0.3 mL of MS-grade water was introduced, and the mixture was incubated again for 10 min at room temperature. After incubation, the samples were centrifuged at 400 rpm at 10 °C for 5 min. The upper organic phase was collected, dried using a speed vac concentrator, and stored at −80 °C. For further lipid analysis, the extract was resuspended in 100 μL of a 65:30:5 (acetonitrile: 2-propanol: water, v/v/v) solution.

3.2. Lipid measurement by LC-MS/MS

Lipid separation was accomplished using an ultra-performance liquid chromatography (UPLC) system equipped with an ACQUITY HSS T3 column (2.1 mm × 100 mm × 1.8 μm, Waters). Solvent A consisted of a 2:3 v/v ratio of water to acetonitrile, and solvent B was a 9:1 v/v ratio of propanol to acetonitrile. The column temperature was maintained at 40 °C with a constant solvent flow rate of 0.3 mL/min. A gradient elution method was applied over an 18-min period, during which solvent B increased from 30 % to 97 % over the first 0–12 min, followed by a 3-min hold. In the final 15.2–18 min, solvent B was returned to 30 %. For data acquisition, a high-resolution mass spectrometer, Orbitrap Fusion (Thermo Scientific, USA), equipped with a heated electrospray ionization source (ESI), was employed. The ESI sheath and auxiliary gases were maintained at 60 and 20, respectively. Both positive and negative spray voltages were set at 3000 V. During the MS run, a resolution of 120,000 with an automatic gain control (AGC) target of 200,000 was utilized, covering a mass range from 250 to 1200. In the subsequent MS/MS runs, the resolution was adjusted to 30,000 with an AGC target of 50,000, and a collision energy of 27 ± 3 was applied for fragmentation.

3.3. Lipid data analysis

Lipid analysis was performed using the LipidMatch Flow software, applying default settings for peak selection (utilizing MZmine), blank filtration, and lipid annotation. Both positive and negative mode data were considered [59]. Subsequently, the MetaboAnalyst software was employed for statistical data analysis. The complete dataset underwent normalization through sum, log-transformation, and pareto scaling before analysis using MetaboAnalyst.

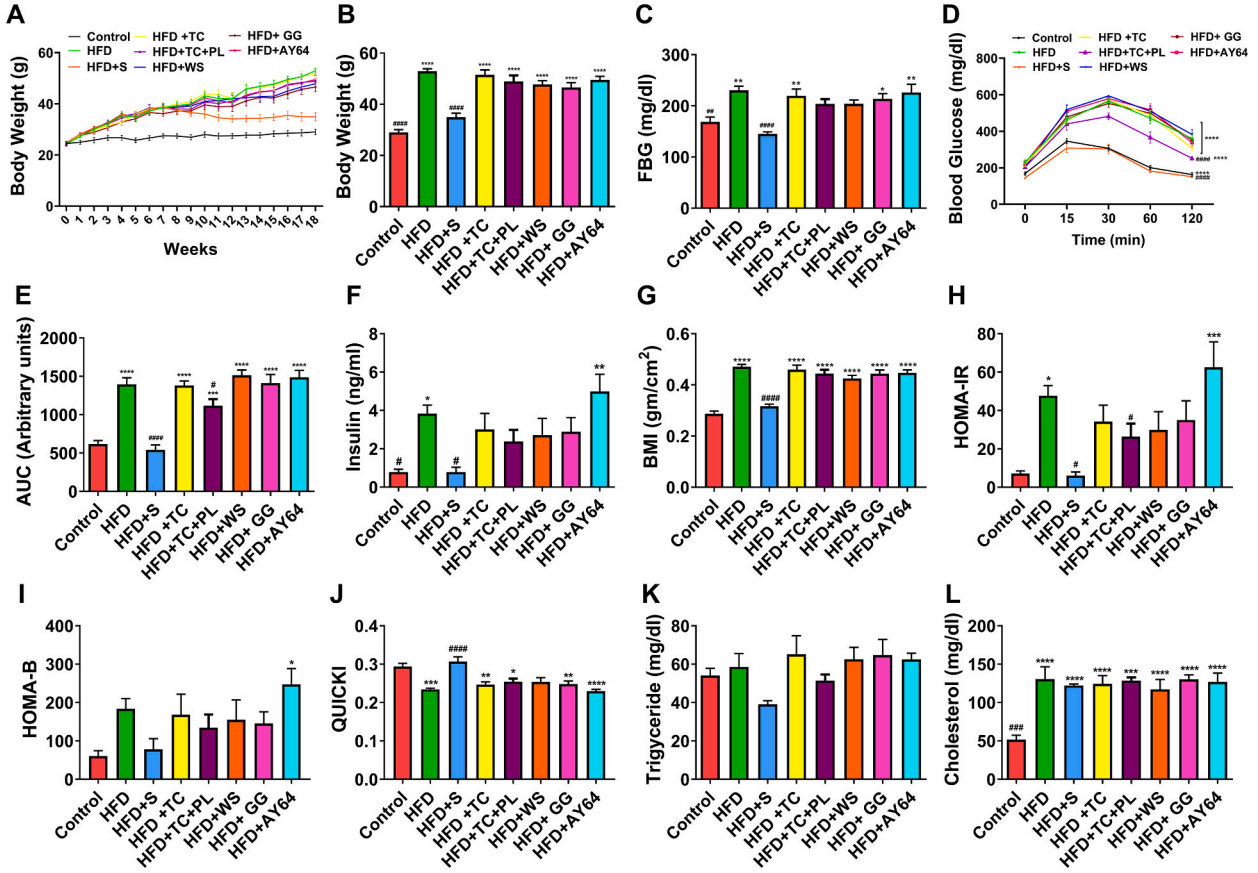

Fig. 1. Effect of herbal extracts and Saroglitazar on the gross and biochemical parameters in mice A) weekly body weight, **B)** average body weights at the end of 18-week, **C)** fasting blood glucose (FBG) levels **D)** Intra-peritoneal glucose tolerance test (IPGTT) after the end of treatment **E)** IPGTT AUC after end of treatment **F)** Insulin, **G)** Body mass index (BMI) **H)** HOMA-IR, **I)** HOMA-B **J)** QUICKI **K)** triglyceride **L)** cholesterol levels, Data are shown as means ± SEM. N = 5–6 per group, $^{*}p < 0.05$; $^{**}p < 0.01$; $^{***}p < 0.001$; $^{****}p < 0.0001$, compared to the control. $^{\#}p < 0.05$; $^{\#\#}p < 0.01$; $^{\#\#\#}p < 0.001$, $^{\#\#\#\#}p < 0.000$, compared to HFD, analyzed via one-way ANOVA followed by Bonferroni's multiple comparisons test. $^{\#}p < 0.05$, compared to HFD, analyzed via Student's t-test for HOMA-IR and AUC.

4. Cell culture studies

4.1. 3D spheroids of HepG2 and LX2 cells

A three-dimensional spheroid model was established by co-culturing two cell lines, HepG2 (hepatocellular carcinoma) and LX2 (hepatic stellate cells), following established protocols [47,60,61].

HepG2 cells were cultured in DMEM (Gibco) with 10 % FBS and 1 % penicillin-streptomycin, while LX2 cells were cultured in DMEM with 2 % FBS and 1 % penicillin-streptomycin. To create the 3D spheroids, a co-culture of HepG2 (2.5 × 103 cells/well) and LX2 (0.5 × 103 cells/well) in DMEM with 10 % FBS and 1 % penicillin-streptomycin (Gibco) was seeded into ultra-low attachment 96-well plates (Corning). The plates were then incubated at 37 °C for 48 h to facilitate the formation of compact, three-dimensional spheroids in each well.

Following this incubation period, the media was replaced with fresh DMEM, and spheroids were treated with Saroglitazar or herbal extracts. Subsequently, they were exposed to palmitic acid (500 μM), and the plates were further incubated at 37 °C in a CO2 incubator for an additional 48 h. After incubation, the plates were centrifuged at 1000×*g* using an Eppendorf centrifuge 5810R. Spheroids were lysed in a lysis buffer, and cDNA was prepared following the manufacturer's protocol (Thermo Fisher). mRNA expression of fibrosis marker genes such as COL1-A1, α-SMA, and TGF-β1 was analyzed via real-time PCR using the TaqMan™ Gene Expression Assay (FAM) (part number 4453320; Applied Biosystems). The internal control 18S was used to normalize gene expression across the wells, employing the TaqMan™ Gene Expression Assay, VIC (Part number 4448489; Applied Biosystems) on a QuantStudio 6 Flex Real-Time PCR System (Applied Biosystems).

4.2. Statistical analysis

The data is presented as means ± SEM (standard error of the mean). For multiple comparisons, we conducted one-way ANOVA or two-way ANOVA (as required), followed by Bonferroni's multiple comparison test using Graph Pad Prism (Version 8.3). For comparisons between two groups, the Student's t-test was employed. A p-value of less than 0.05 was considered statistically significant.

5. Results

5.1. Effects of herbal extracts and Saroglitazar on gross, and biochemical parameters in HFD fed mice

To assess the effects of herbal extracts and Saroglitazar, we utilized a mouse model of obesity, IR, and fatty liver induced by HFD comprising 60 kcal% (closer to a Western diet). Over an 18-week period, HFD-fed mice demonstrated progressive weight gain in comparison to control mice fed a standard chow diet (Fig. 1A and B). Following 6 weeks of HFD feeding, we initiated a 12-week treatment regimen with TC, TC + PL, WS, GG, and AY-64, which did not significantly alter the weight gain compared to the HFD group (Fig. 1A and B). In contrast, mice treated with Saroglitazar for 12 weeks showed a significant reduction in body weight (Fig. 1A and B). Moreover, 18 weeks of HFD feeding resulted in the development of IR and hyperglycemia. Treatment with TC, TC + PL, WS, GG, and AY-64 did not significantly affect fasting blood glucose levels when compared to the HFD group (Fig. 1C). However, Saroglitazar-treated mice exhibited a significant reduction in fasting blood glucose levels (Fig. 1C). To evaluate the impact of the HFD on glucose tolerance and insulin sensitivity, an intraperitoneal glucose tolerance test (IPGTT) was conducted at the end of 18 weeks. The HFD group displayed impaired glucose tolerance (Fig. 1D and E), while Saroglitazar treatment reversed the increase in glucose levels (Fig. 1D and E). TC + PL treatment for 12 weeks also demonstrated a significant improvement in glucose intolerance, whereas TC, WS, GG, and AY-64 treatments did not improve glucose intolerance, as indicated by the AUC levels (Fig. 1E). Consistent with the glucose levels, plasma insulin levels were significantly elevated in the HFD group mice (Fig. 1F). Saroglitazar ($p < 0.05$) and TC + PL ($p < 0.085$, ~38 %) reduced plasma insulin levels compared to the HFD group.

Additionally, we assessed BMI at the end of the 18-week treatment period (Fig. 1G), which is used as a screening tool for overweight/obesity. Increased BMI was observed in the HFD-fed group compared to the chow-fed control group (Fig. 1G), and this increase was mitigated by Saroglitazar treatment. However, all the herbal extracts had no effect on BMI compared to the HFD group. Increased HOMA-IR, HOMA B, and decreased QUICKI (Fig. 1H–J) values in the HFD group confirmed the presence of IR. HOMA-IR values were significantly reduced in the Saroglitazar and TC + PL groups, whereas TC, GG, WS, and AY-64 had no significant effect compared to the HFD group (Fig. 1H). The HOMA B value was also reduced following Saroglitazar treatment, while all the tested extracts did not show any significant effect compared to the HFD group (Fig. 1I). QUICKI values were significantly increased following Saroglitazar treatment, but none of the tested extracts had an impact on QUICKI values compared to the HFD group (Fig. 1J).

IR is also associated with elevated TG, abnormal cholesterol profiles, and alterations in other lipid species. Therefore, we also assessed plasma TG and total cholesterol levels among the groups. Fig. 1K illustrates the changes in plasma TG levels among the groups at the end of 18 weeks. TG levels remained unchanged in the control and HFD-fed groups. Saroglitazar treatment for 12 weeks led to a reduction in plasma TG levels compared to the control and HFD-fed mice, although these changes did not reach statistical significance. Moreover, treatment with TC, TC + PL, WS, GG, and AY-64 for 12 weeks did not result in any significant alterations in plasma TG levels. Next, we evaluated plasma cholesterol levels among the groups (Fig. 1L). Feeding an HFD for 18 weeks significantly increased plasma cholesterol content ($p < 0.001$). Treatment with Saroglitazar, TC, WS, GG, AY-64, and TC + PL for 12 weeks did not induce any significant changes in plasma cholesterol levels compared to the HFD group (Fig. 1L).

5.2. The effect of herbal extracts and Saroglitazar on liver weight and the gene expression of inflammatory cytokines

Lipid accumulation and tissue inflammation are associated with an increase in liver weight. The HFD-fed group exhibited a significantly higher absolute liver weight ($p < 0.001$) at the end of 18 weeks in comparison to the control group (Fig. 2A). There were no significant changes in liver weight observed between the Saroglitazar, TC, WS, GG, and AY-64 treated groups when compared to the HFD-fed group. Treatment with TC + PL, however, resulted in a significant reduction in liver weight ($p < 0.05$, approximately a 32 % reduction compared to the HFD group) (Fig. 2A). When assessing the liver-to-body weight ratio, no significant changes were observed between the control and HFD groups. However, compared to the control group, the liver-to-body weight ratio was significantly increased in the Saroglitazar-treated group (Fig. 2B). We did not find any significant differences between the groups compared to the HFD group (Fig. 2B).

We also assessed the expression of key cytokines involved in inflammation (see Fig. 2C–G). The expression of the pro-inflammatory cytokine, *IL-1β* (Fig. 2C), demonstrated an increasing trend in the HFD group (approximately 2.4-fold) and in all the treated groups when compared to the control group. Furthermore, there was a notable ~40 % decrease in *IL-1β* expression in the TC + PL group compared to the TC-treated group. No significant differences were observed in the expression of *IL-6* between the HFD group and the treated groups (Fig. 2D). Additionally, we examined the expression of *TNF-α* (Fig. 2E). An increasing trend (~2.4-fold) in *TNF-α* expression was observed in the HFD group compared to the control group, although it did not reach statistical significance. In contrast, Saroglitazar treatment significantly increased *TNF-α* expression compared to both the control and HFD groups. The expression of *TNF-α* in the groups treated with TC, WS, GG, and AY-64 remained comparable to that in the HFD group. The TC + PL group showed a significant reduction in *TNF-α* expression (~71 % decrease compared to the HFD and 72 % decrease compared to the TC group). No significant differences were observed in the expression of *IL-4* between the HFD and control groups (Fig. 2F). The expression of *IL-4* in the Saroglitazar, TC, and GG-treated groups remained comparable to that in the HFD group. Groups treated with WS, AY-64, and TC + PL displayed reductions in *IL-4* expression, although the reductions were statistically not significant, except in the TC + PL group (~71 % and 72 % decreases compared to the HFD and TC groups, respectively). An increasing trend in the expression of *IL-10* was observed in the HFD group, as well as in the Saroglitazar, TC, WS, GG, and AY-64 groups compared to the control group (Fig. 2G). The expression of IL-10 in the TC + PL-treated group remained comparable to the control group. Additionally, a decrease of ~67 % and ~78 % in *IL-10* expression was observed in the TC + PL-treated group compared to the HFD and TC-treated groups, respectively.

5.3. Impact of herbal extracts and Saroglitazar on HFD-induced lipid accumulation and hepatic tissue histological alterations

Hepatic lipid accumulation is a critical process in the development of NAFLD, which is closely associated with IR. The microscopic evaluation of liver inflammation and steatosis was conducted using H&E staining (Fig. 3A, upper panel) and ORO staining (Fig. 3A, lower panel), respectively. In the upper panel of Fig. 3A, the control group displayed a normal cell structure with no evidence of

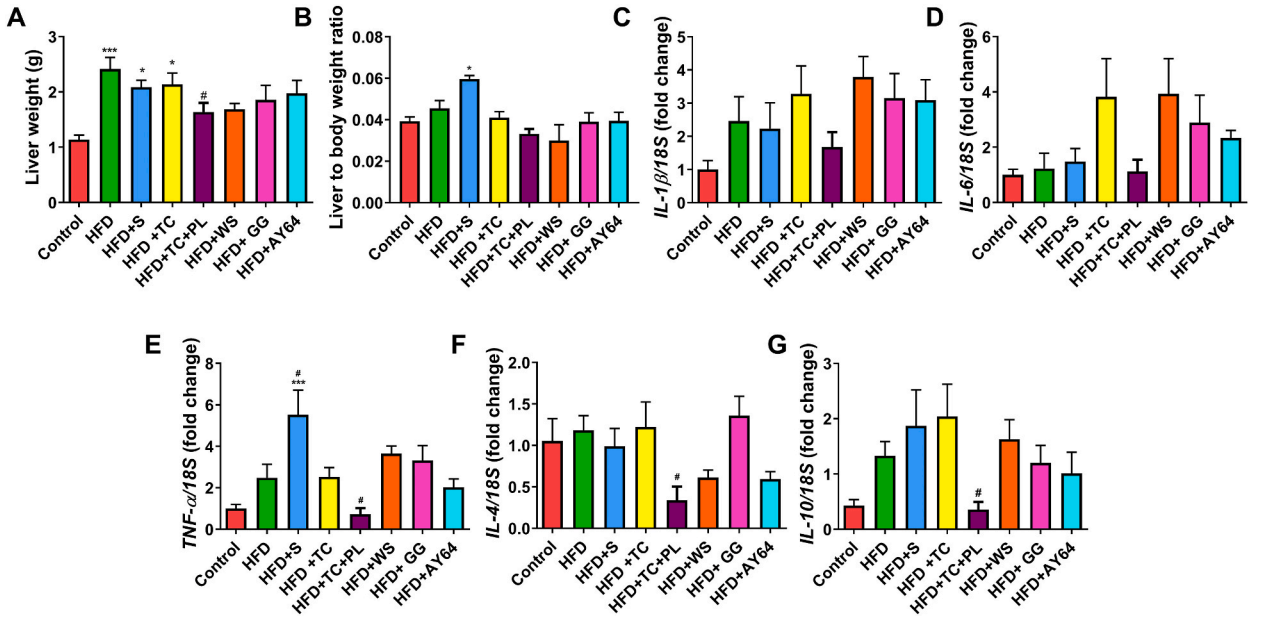

Fig. 2. Impact of herbal extracts and Saroglitazar on liver weight and the mRNA expression levels of inflammatory cytokines. A) liver weight, **B)** Liver/body weight ratio, total RNA was isolated using TRIzol reagent from the hepatic tissues. Shown are fold-changes of expression normalized to 18S rRNA expression; **C)** *IL-1β*; **D)** *IL-6*; **E)** *TNF-α*; **F)** *IL-4*; **G)** *IL-10*. Data are shown as mean ± SEM. N = 3–6 per group $^{*}p < 0.05$; $^{***}p < 0.001$, compared to control analyzed via one-way ANOVA followed by Bonferroni's multiple comparisons test. $^{\#}p < 0.05$, compared to HFD, analyzed via Student's t-test.

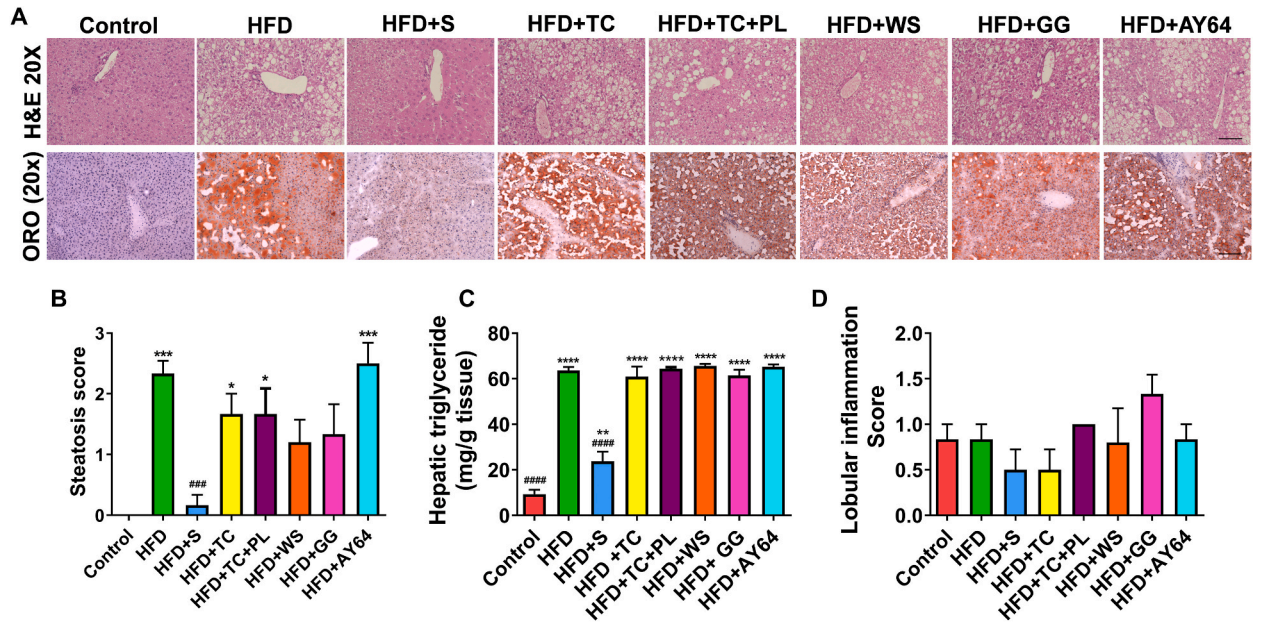

Fig. 3. Influence of herbal extracts and Saroglitazar on the HFD induced lipid accumulation and histological changes in the hepatic tissue, A) Representative photographs of liver tissue sections; H&E stain in the first lane, ORO stain in the second lane, magnification at 20×; **B)** Steatosis Score, **C)** Hepatic TG accumulation, **D)** Lobular inflammation score. N = 5–6 per group, Data are shown as means ± SEM.*$p < 0.05$; **$p < 0.01$; ***$p < 0.001$; ****$p < 0.0001$, compared to the control analyzed via one-way ANOVA followed by Bonferroni's multiple comparisons test. Scale bars represent 200 μm.

macrovesicular or microvesicular steatosis, ballooning, or inflammatory cell infiltration. ORO staining, a selective fat-soluble stain for neutral triglycerides and lipids, revealed an increase in ORO-stained droplets and inflammatory cell infiltration in the liver sections of the HFD group (Fig. 3A, lower panel). Histological scoring confirmed significantly enhanced fat accumulation inside hepatocytes, referred to as macrovesicular steatosis (Fig. 3B). In contrast, the liver histology after 12 weeks of Saroglitazar treatment showed a reduction in lipid accumulation, although mild steatosis was still evident (Fig. 3A and B). Treatment with TC, TC + PL, WS, GG, and AY-64 for 12 weeks did not result in a significant reduction in lipid accumulation (Fig. 3A). However, TC and TC + PL treatment displayed an approximate 30 % decrease in the steatosis score compared to the HFD group (Fig. 3B). GG and WS also showed a decreasing trend in the steatosis score compared to the HFD group (Fig. 3B). To validate these observations, we also measured the hepatic TG content in all the groups. Fig. 3C displays the hepatic TG content after 18 weeks of control diet or HFD treatments. Hepatic TG levels were significantly higher in the HFD-fed group compared to the control group ($p < 0.001$). Saroglitazar treatment for 12 weeks significantly reduced hepatic TG levels ($p < 0.001$) compared to the HFD group. Treatment with TC, TC + PL, WS, GG, and AY-64 after 12 weeks did not alter the hepatic TG content compared to the HFD-treated mice group. No significant changes were observed in the lobular inflammation scoring among all the groups (Fig. 3D).

5.4. Influence of herbal extracts and Saroglitazar on gene expression related to hepatic lipid metabolism and bile acid synthesis

The HFD group exhibited increased lipid accumulation, as evidenced by ORO staining and histological analysis. Consequently, we evaluated the mRNA expression of genes related to lipid metabolism and bile acid synthesis (Fig. 4). In the HFD group, there was an upregulation of approximately 5-fold and 3-fold in the mRNA expression of PPAR-γ and SREBP-1c, respectively, compared to the control group (Fig. 4A and B). Saroglitazar treatment resulted in a reduction in PPAR-γ expression, while there was a slight increase in the expression of SREBP-1c compared to the HFD group. The mRNA expression of PPAR-γ in the TC-treated group remained comparable to that of the HFD group; however, the expression of SREBP-1c was significantly increased compared to both the control and HFD groups. In contrast, the TC + PL treated group showed mRNA expressions of PPAR-γ and SREBP-1c comparable to the HFD group. Moreover, when compared to the TC-treated group, TC + PL displayed a reduction of approximately 33 % in the mRNA expression of PPAR-γ and 44 % in the mRNA expression of SREBP-1c (Fig. 4A and B). The WS-treated group exhibited an increasing trend in the expressions of PPAR-γ and significant upregulation of SREBP-1c compared to the HFD group (Fig. 4A and B). In the GG and AY-64 treated groups, no significant changes were observed in the expressions of PPAR-γ and SREBP-1c when compared to the HFD group (Fig. 4A and B).

The expression of FABP-1 (fatty acid binding protein-1) remained unchanged when compared to the HFD group (Fig. 4C). However, it was significantly upregulated in the WS and AY-64 treated groups compared to the control group. We also analyzed the mRNA expression of CD36 (Fig. 4D), a gene involved in fatty acid translocation and uptake. After 18 weeks of HFD feeding, CD36 mRNA expression was significantly upregulated (~29-fold) in the hepatic tissue of the HFD group. Statistically, there were no significant

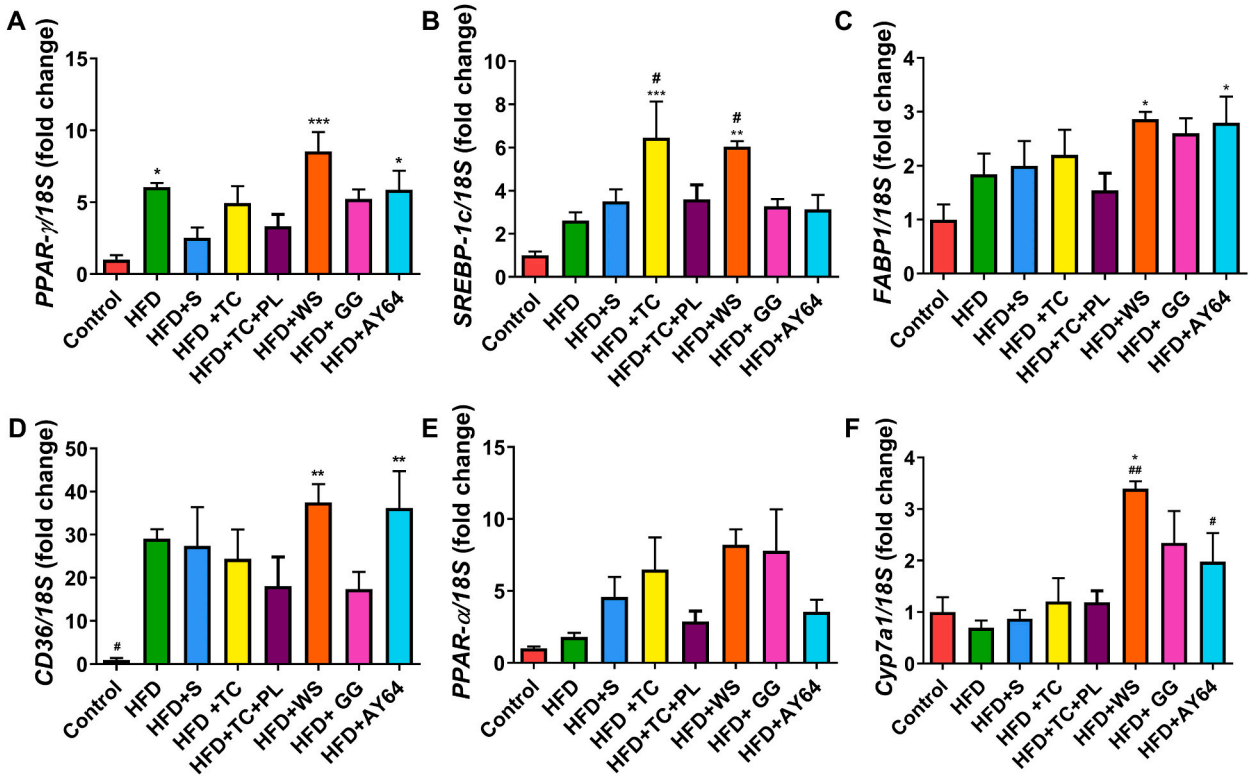

Fig. 4. Modulation of the expression of lipid metabolism related genes following treatment with herbal extracts and Saroglitazar. Total RNA was isolated using TRIzol reagent from the hepatic tissues. qPCR data from mRNA extraction of liver tissues. Shown are fold-changes of expression normalized to 18S rRNA expression. Expression of genes involved in lipid metabolism **A)** *PPARγ*, **B)** *SREBP-1c*, gene involved in transport; **C)** *FABP1* **D)** *CD36*, genes involved in fatty acid oxidation; **E)** *PPAR-α* and gene involved in bile acid synthesis; **F)** *Cyp7a1* N = 3–6 Data are shown as means ± SEM. $^{*}p < 0.05$; $^{**}p < 0.01$; $^{***}p < 0.001$; compared to control. $^{\#}p < 0.05$, $^{\#\#}p < 0.01$, $^{\#\#\#}p < 0.001$ compared to HFD analyzed via one-way ANOVA followed by Bonferroni's multiple comparisons test.

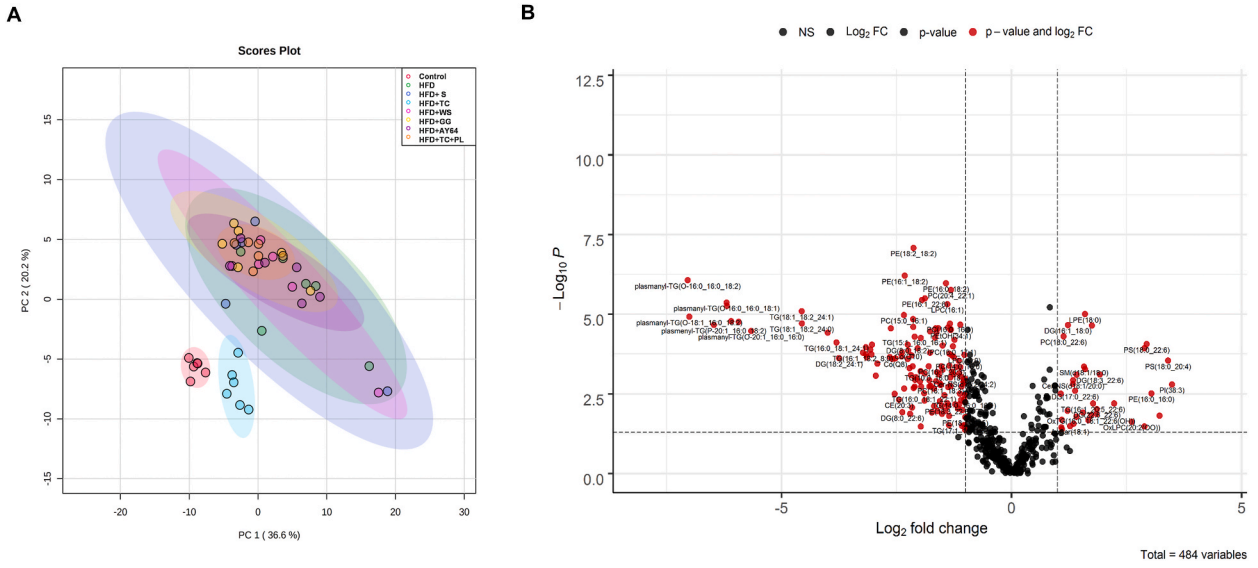

Fig. 5. Effect of herbal extracts and Saroglitazar on lipid profiling in the liver. A) 2D score plots of principal component analysis (PCA) among Control, HFD, HFD + S, HFD + TC, HFD + WS, HFD + GG and HFD + AY-64 and HFD + TC + PL groups, at end point in hepatic lipids. **B)** Volcano plot between the Control and HFD groups.

changes in CD36 mRNA expression between Saroglitazar, TC, TC + PL, WS, GG, and AY-64 when compared to the HFD group. However, the TC + PL and GG-treated groups displayed a slight decrease of 38 % and 40 %, respectively, in comparison to the HFD group. There was also a decrease of approximately 26 % in CD36 mRNA expression in the TC + PL group when compared to the TC group. Next, we assessed the expression of the fatty acid oxidation marker PPAR-α among the groups (Fig. 4E). Although not statistically significant, PPAR-α expression remained higher in the HFD group (approximately 2-fold) compared to the control group. Treatment with Saroglitazar, TC, WS, and GG showed an increasing trend in PPAR-α expression, but it did not reach statistical significance. PPAR-α expression was lower in the TC + PL and AY-64 treated groups compared to the other treatment groups, with the TC + PL group showing a reduction of about 56 % compared to the TC group (Fig. 4E).

Subsequently, we examined the mRNA expression of CYP7a1, a gene involved in bile acid synthesis (Fig. 4F). The expression of CYP7a1 remained unchanged between the control, HFD, Saroglitazar, TC, and TC + PL groups. However, it was significantly upregulated in the WS and AY-64 treated groups compared to the HFD group. Treatment with GG also exhibited an increasing trend in CYP7a1 expression compared to the control or HFD group, although it did not reach statistical significance.

5.5. *Impact of herbal extracts and Saroglitazar on hepatic lipid species profile*

We conducted a comprehensive lipidome analysis of hepatic tissues from all study groups to investigate changes in lipid species associated with IR. An untargeted lipid profiling approach was employed using Orbitrap Fusion mass spectrometry coupled with UPLC,

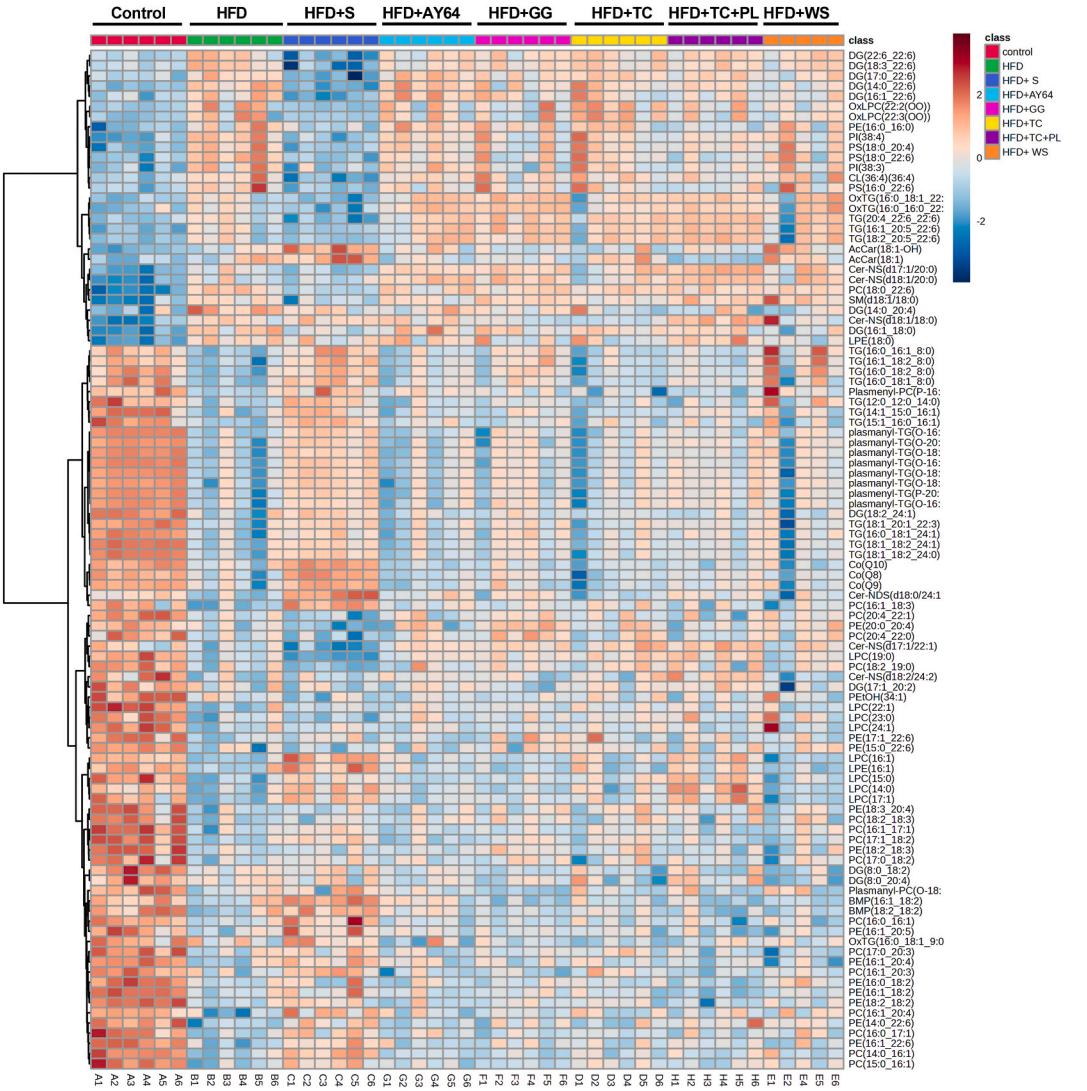

Fig. 6. Heat map of differential lipids among Control, HFD, HFD + S, HFD + TC, HFD + WS, HFD + GG and HFD + AY-64 and HFD + TC + PL groups at the end point. N = 5–6 per group. Hot (red) colour and cool (blue) colour indicates increased and decreased levels of lipids, respectively.

which identified a total of 484 lipids. The PCA plot (Fig. 5A) clearly distinguishes between the control and HFD groups. Principal components 1 and 2 explained 37 % and 20 % of the data, respectively, suggesting significant alterations in the lipidome across the study groups. The volcano plot (Fig. 5B) highlights differential lipid species between the control and HFD groups. To further analyze the variation in the expression of the top 100 significantly altered hepatic lipids among the eight groups, we generated a cumulative heat map (Fig. 6). Saroglitazar treatment in the HFD-fed animals reversed 54 lipids, bringing them back to levels similar to the control group. Statistical comparisons revealed that the herbal extracts TC, WS, GG, and AY-64 had less pronounced effects on the lipid profiles in the HFD model. However, the combination of TC + PL had a significant modulating effect on the lipid profile in the HFD group. To confirm the identified differential lipids in hepatic tissues, we performed cluster analysis and selected the top 25 lipids to generate a hepatic lipid heatmap. The heat map showed a significant reduction in the levels of saturated TGs in the HFD group compared to the control group, as observed in our previous study [39]. Most of these TGs were restored in the HFD + TC + PL group (Fig. 7H-M). The same trend of increment was observed in other lipids such as ceramide-NS (d18:2/24:2), lysophosphatidylcholines (LPC) (14:0, 16:1, and 17:1) (Fig. 7B, D-F). Following treatment with TC + PL, the abundance of these lipids was reversed to levels similar to the control group. Lipids such as acylcarnitine (AcCar) (18:1), diglyceride (DG) (14:0_20:4), and phosphatidylinositol, PI (36:4) increased nearly two-fold in the liver of the HFD group compared to the control group, as reported in our previous study (Fig. 7A, C, & G). The HFD + TC + PL group displayed levels of these lipids similar to the control group, suggesting a therapeutic action of TC + PL. This was further supported by the box plots generated from the data (Fig. 7, Data S2).

5.6. *Effect of herbal extracts and Saroglitazar on liver fibrosis*

Masson's Trichrome (MT) staining in liver tissue sections of all groups reveals comparable levels of collagen deposition around the portal veins (Fig. 8A). The overall NAS score remains higher in the HFD group (Fig. 8B). No significant differences are observed in the NAS score between the groups treated with Saroglitazar, TC, TC + PL, WS, GG, and AY-64. Furthermore, we assessed the mRNA expressions of genes related to fibrosis (Fig. 8C–G). Despite no visible differences in histopathological staining, the HFD group liver showed upregulated mRNA expression of fibrosis-related markers: approximately 7-fold for *TGF-β1*, 17-fold for *COL1A1*, 6-fold for *α-SMA*, 17-fold for *TIMP-1*, and 5-fold for *MMP2*, compared to the control group (Fig. 8C–G). Treatment with Saroglitazar indicates a trend of increased mRNA expression for *TGF-β1*, *COL1A1*, and *MMP2*, while *α-SMA* expression remained comparable to the HFD group. In the TC-treated groups, mRNA expression of *COL1A1*, *α-SMA*, and *MMP2* is comparable to the HFD group. Although not statistically

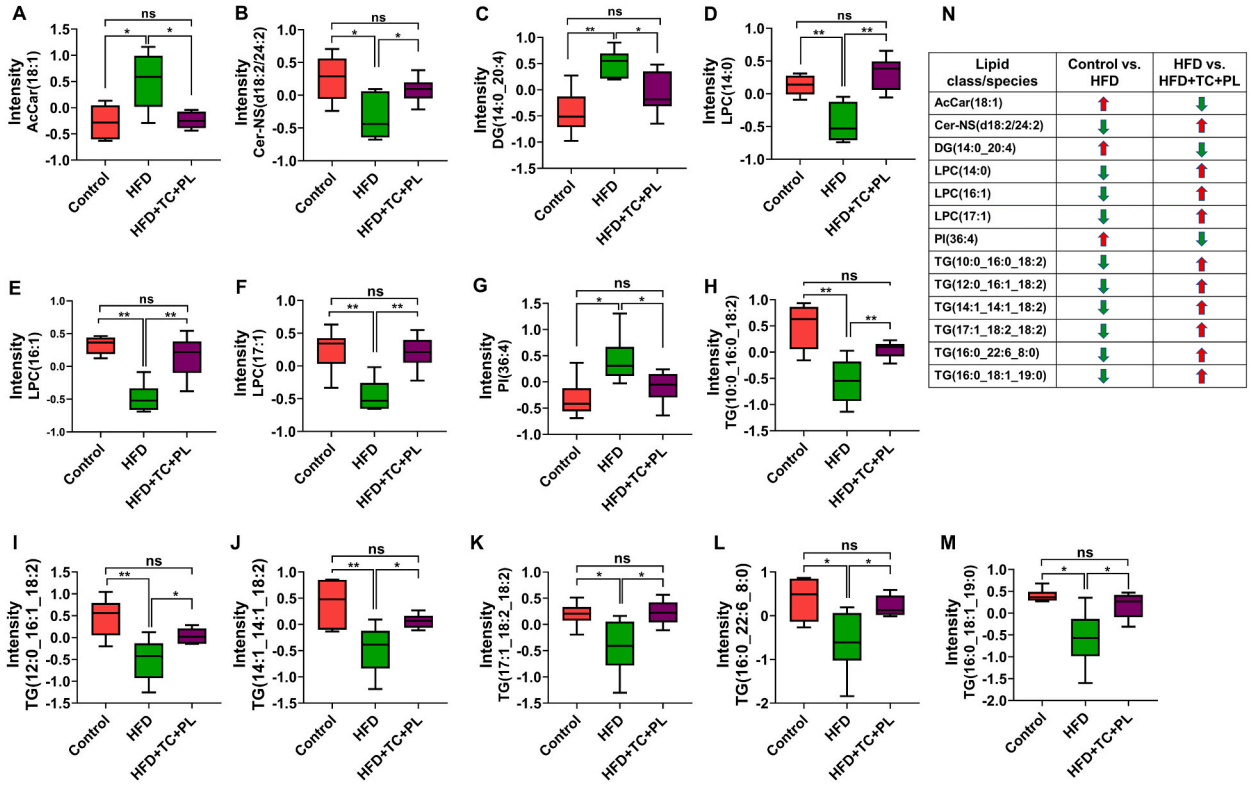

Fig. 7. Abundance of selected lipid species by box plots between control, HFD and HFD + TC + PL groups. Box plots of **A)** acylcarnitines (AcCAR), **B)** sphingosine containing ceramides (Cer-NS), **C)** diacylglycerol (DAG), **D-F)** lysophosphatidylcholines (LPC), **G)** phosphatidylinositol (PI) and **H-M)** triglycerides (TG). The middle line in the box equals the median value, the tops and bottom lines are the first and third quartile. **N)** Demonstration of changes in lipids upregulation (↑)/downregulation (↓).

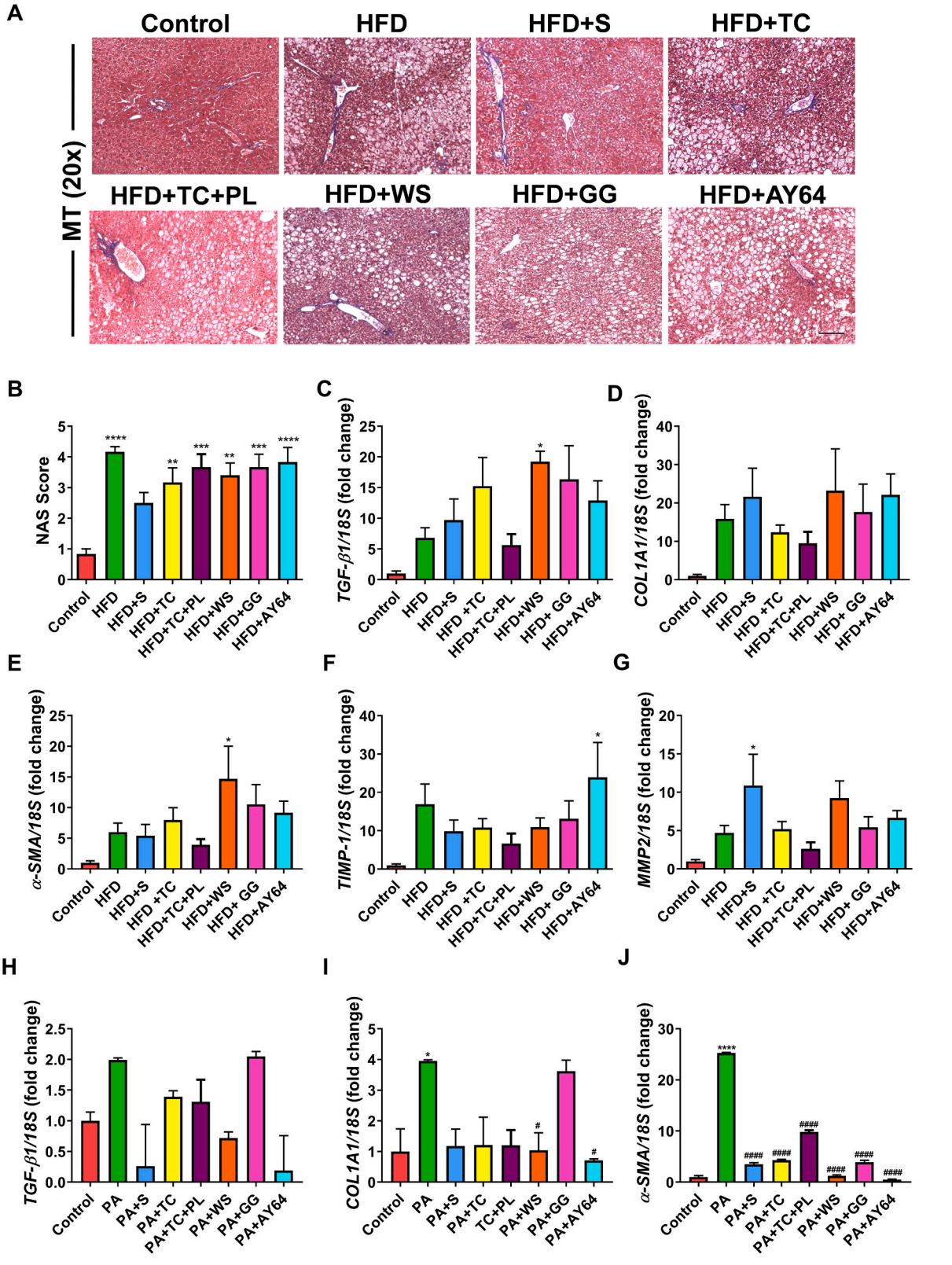

(caption on next page)

Fig. 8. Effect of herbal extracts and Saroglitazar on liver fibrosis. Representative photographs for **A)** MT staining, magnification at 20×; **B)** NAS score. qPCR data from mRNA extraction of liver tissues. Shown are fold-changes of expression normalized to 18S rRNA expression **C)** *TGF-β1*; D) *COL1A1*; **E)** *α-SMA*; **F)** *TIMP*-1; **G)** *MMP2*. Data are shown as means ± SEM. N = 3–6, $^{*}p < 0.05$; $^{**}p < 0.01$; $^{***}p < 0.001$; $^{****}p < 0.0001$ compared to control. qPCR of hepatic 3D-speroids from Co-culture of HepG2 and LX2 cells. Shown are fold-changes of expression normalized to 18S rRNA expression. **H)** *TGF-*β1; **I)** *COL1* A1; **J)**. *α-SMA*. N = 3, $^{*}p < 0.05$, $^{**}p < 0.01$, $^{***}p < 0.001$ compared to control. $^{\#}p < 0.05$, $^{\#\#\#\#}p < 0.0001$, compared to HFD/PA (Palmitic acid) analyzed via one-way ANOVA followed by Bonferroni's multiple comparisons test. Scale bars represent 200 μm.

significant, *TGF-β1* expression slightly increased, and *TIMP-1* expression slightly decreased compared to the HFD group. In the TC + PL treated group, expression of all fibrosis-related markers is reduced: *TGF-β1* (~18 % and 63 %), *COL1A1* (~40 % and 23 %), *α-SMA* (~34.3 % and 51 %), *TIMP-1* (~61 % and 37 %), and *MMP2* (~44 % and 49 %), compared to either the HFD group or the TC-treated groups, respectively. However, these changes are not statistically significant. The expression of all fibrosis-related marker genes in the WS, GG, and AY-64 treated groups remained higher compared to the control group and showed an increase or no change compared to the HFD group (Fig. 8C–G).

5.7. Influence of herbal extracts and Saroglitazar on palmitic acid (PA)-induced fibrosis in a 3D spheroid hepatic co-culture model

Since we only observed changes in gene expression in the mouse model without significant alterations in histological assessments, we conducted experiments in 3D spheroids to validate our findings. Treatment of 3D spheroids with PA (500 μM) resulted in an increase in the mRNA levels of fibrosis markers, such as *TGF-β1*, *COL1A1*, and *α-SMA* (Fig. 8H–J). To validate the model, we employed Saroglitazar (10 μM), a positive control known for its efficacy, which reduced the expression of these fibrosis markers, consistent with previous findings in a co-culture model using HepG2 and LX2 cells [60].

Furthermore, all the extracts used in the study reduced the PA-induced expression of *α-SMA*. TC, TC + PL, WS, and AY-64 reduced the PA-induced expression of *α-SMA* and *COL1A1* (Fig. 8J and I). However, only WS and AY-64 attenuated the PA-induced expression of *TGF-β1* (Fig. 8H). TC and TC + PL also exhibited moderate inhibition of PA-induced *TGF-β1* expression (Fig. 8H). In contrast, GG failed to reduce the mRNA levels of *COL1A1* and *TGF-β1*, unlike *α-SMA* (Fig. 8H–J).

6. Discussion

In this study, we utilized a diet-induced murine model of IR and an in vitro hepatic 3D spheroid model to investigate the impact of select herbs on obesity, IR, and the expression of inflammatory and fibrotic genes. Additionally, we analyzed the effects of these herbs and Saroglitazar on key hepatic lipid species after 12 weeks of treatment. The herbal extracts used in this study gained prominence during the COVID-19 pandemic due to their potential to prevent SARS-CoV-2 infection and associated complications [34,62,63]. Individuals with T2DM are particularly susceptible to infections, leading to adverse outcomes associated with these comorbidities [64]. Previous research from our lab has highlighted the protective effects of these herbal extracts in SARS-CoV-2 experimental models, attributed to their modest antiviral activity and immunomodulatory properties [49–52].

Weight gain and obesity are significant contributors to metabolic disorders, including IR, T2DM, NAFLD, and atherosclerosis [65]. Our study involved feeding mice 60 % HFD for 18 weeks, resulting in substantial body weight gain compared to control mice fed a standard chow diet. The herbal extracts employed in this study possess diverse biological activities and are in common human use. Hence, they were administered at human equivalent doses to evaluate their effectiveness against obesity, IR, and the expression of inflammatory and fibrotic genes in the aforementioned models. Consistent with previous reports, Saroglitazar significantly reduced body weight gain in HFD-fed mice [46,66]. However, the herbal extracts did not lead to any significant changes in body weight. Beyond weight reduction, improvements in IR, dyslipidemia, and inflammation are critical in mitigating T2DM. Among the extracts used in this study, only the TC + PL combination exhibited modest protection against HFD-induced IR, inflammation, and dyslipidemia. TC alone did not reverse HFD-induced obesity or associated changes. In our previous lab study, PL alone also did not demonstrate a beneficial effect on the parameters investigated (unpublished data). Combining TC with PL enhanced the bioavailability and antioxidant capacity of TC [67–69]. Additionally, piperine, a major alkaloid and active constituent of Piper longum Linn, is known to enhance the bioavailability of nutraceuticals and drugs [70]. Piperine also promotes glutathione production and transport while replenishing thiol levels by inhibiting lipid peroxidation [71]. These effects, however, were not consistently reflected in some biochemical and histological parameters but were more pronounced at the hepatic lipidome level, suggesting that changes in hepatic lipid species may precede clinical parameters, as observed by others [72]. The remaining herbal extracts failed to exhibit protective effects in the DIO model. Seasonality and extraction methods could be the reason of the effects observed with the extracts in this study. As seasonal variations significantly affect a plant's life cycle, and their phytochemical content [73]. Furthermore, extraction methods and techniques also influence the phytochemical content and bioactivity of plant extracts [74]. Previous research indicates that factors such as extraction temperature and solvent choice impact the yield of phenolic content and the antioxidant capacity of medicinal plants [73,75]. It is to be noted that the present study employed aqueous herbal extracts, while organic extraction methods have been shown to enhance phytochemical constituents [73]. Although these extracts reduced α-SMA expression in the in vitro 3D spheroid model, the literature suggests variable effects of some of these extracts on inflammation and T2DM in different models, depending on treatment duration and doses [12–15,18,42,22–27]. For future studies, a dose-response investigation of these herbal extracts using relevant models of steatosis, inflammation, and fibrosis would provide a clearer understanding of their potential benefits against IR, inflammation, fibrosis, and fatty liver associated with T2DM.

Significant changes in inflammatory cytokines can lead to systemic IR, which is also detrimental for fatty liver disease progression [76,77]. TNF-α, a proinflammatory cytokine, and IL-10, an anti-inflammatory cytokine, play roles in regulating systemic IR [78]. TC + PL treatment reversed TNF-α and IL-10 expression, potentially indicating a reduction in inflammation due to the decrease in liver weight. In contrast to other studies, we observed increased mRNA expression of TNF-α in the hepatic tissue of Saroglitazar-treated animals compared to the chow diet and HFD-fed groups, consistent with our previous findings [46]. IL4 exhibits both pro and anti-inflammatory effects [79,80]. In the HFD + TC + PL group, IL-4 mRNA expression significantly decreased. IL-4 has been shown to reduce lipid accumulation by promoting hormone-sensitive lipase (HSL) activity [81]. Recent studies indicate that IL-4 functions as a type 2 cytokine in tissues, aiding in collagen production and extracellular matrix deposition. Thus, the reduction in IL-4 expression in the HFD + TC + PL group may be beneficial in preventing NASH-induced fibrosis [82,83]. However, further investigation is needed to assess changes in mRNA expression at the protein level. Multiple clinical trials have highlighted anti-inflammatory potential of herbs and their ability to improve IR [84]. Alongside inflammation, we observed impaired glucose tolerance and IR in HFD-fed mice. Both Saroglitazar and TC + PL treatments improved glucose tolerance and insulin sensitivity. Although insulin levels were not significantly reduced, HOMA-IR results suggest improved insulin sensitivity in the TC + PL treated group. Additionally, a trend of decreased HOMA-B indicates improved β-cell function in the TC + PL treated group.

Peripheral IR, obesity-induced inflammation, and dyslipidemia often lead to fatty liver, which is associated with T2DM [85]. Histological analysis, however, showed that, unlike Saroglitazar, herbal extracts did not mitigate steatosis. CD36, a free fatty acid (FFA) transporter gene, was upregulated by ~29-fold in the HFD-fed group, consistent with previous observations [86]. A study in HFD-fed mice demonstrated that hepatocyte-specific disruption of CD36 improved fatty liver states and insulin sensitivity [87]. Though not statistically significant, TC + PL and GG treatment exhibited a trend of decreased CD36 expression. Hepatic PPAR-γ plays a significant role in regulating glucose and lipid metabolism and is involved in hepatic steatosis development [88,89]. We also observed increased expression of hepatic PPAR-γ and SREBP-1c in HFD-fed mice. Liver-specific deletion of PPAR-γ in ob/ob mice reduced hepatic lipid accumulation [90]. Similarly, SREBP-1c overexpression in the liver has been associated with the progression of fatty liver [91]. Both Saroglitazar and TC + PL treatment showed a trend of decreased PPAR-γ expression. Saroglitazar and some of the herbal extracts used had no effect on SREBP-1c expression, whereas TC and WS treatment significantly increased SREBP-1c expression.

Most extracts used in this study possess antioxidant activity, which is associated with reduced liver fibrosis [92]. TC + PL showed a trend of decreasing fibrosis gene markers, specifically COL1A1, TIMP-1, and MMP2. TIMP-1 contributes to diet-induced hepatic steatosis development, as seen in TIMP-1 knockout mice on an HFD that gained less weight, improved glucose tolerance, and reduced hepatic steatosis [93]. Notably, TC + PL treatment also reduced TIMP-1 expression in HFD-fed mice. The role of MMP2 is contradictory, as MMP2 null mice showed increased fibrosis, indicating a protective role rather than a pathogenic one [94–96]. In our study, MMP2 expression significantly increased after HFD feeding, including in the Saroglitazar and WS treatment groups, while TC + PL treatment reduced MMP2 expression. A previous study in HFD-fed rodents reported a significant induction in MMP2 levels along with fibrosis [97]. Our study observed increased MMP2 expression after HFD feeding, including in the Saroglitazar and WS treatment groups, while TC + PL treatment reduced MMP2 expression. A prior study in HFD-fed rodents similarly reported elevated MMP2 levels along with fibrosis.

In the context of lipid research, unique lipid species accumulating in hepatic tissue are recognized for their roles in IR and inflammation [98,99]. To comprehensively assess the protective effects of Saroglitazar and TC + PL in a 3D culture model and HFD-fed mice, we employed an untargeted lipidomic approach. In the HFD + TC + PL group, we identified 13 lipids with aberrant levels compared to the control group. Notably, TC + PL treatment normalized AcCar (18:1) levels, which remained elevated with other herbal extracts. High AcCar levels have been associated with human hepatocellular carcinoma (HCC) and have been observed in the serum and liver of HFD-fed mice [39,100]. Serra et al. demonstrated that abnormal AcCar retention and impaired fatty acid clearance contribute to steatosis-induced hepatic inflammation [101].

Additionally, Saroglitazar, TC, and TC + PL effectively prevented the ectopic accumulation of DAGs. Previous studies have linked DAG buildup to IR and glucose toxicity in uncontrolled T1DM or T2DM. DAG activates PKCε, which directly inhibits insulin receptor tyrosine kinase activity by binding to it, resulting in hepatic IR [102,103]. Recent studies have also revealed that the hepatic abundance of DAGs increases the risk of IR and significantly raises the incidence of cirrhosis [104,105]. The combination of TC + PL reduced hepatic DAG levels, which may contribute to improved IR in HFD-fed mice.

Lipotoxicity in the liver is linked to an increase in saturated TGs and a decrease in unsaturated TGs (containing PUFA) [106]. Saroglitazar, TC + PL, and GG significantly improved unsaturated TG levels, which were reduced in the HFD group. Elevated PI levels in hepatocytes trigger PI3K overexpression, inducing autophagy and hepatic inflammation [107]. Unlike most herbal extracts, TC + PL reduced PI (36:4) levels, potentially reducing inflammation.

LPCs are proinflammatory and play a role in cholesterol metabolism [108]. Their function depends on the attached fatty acid (FA) moiety [109], with some inducing inflammation. In cirrhotic patients, LPC (14:0) and LPC (16:1) levels are elevated [110]. TC + PL normalized LPC levels, reducing the expression of inflammatory markers. Ceramide-NS, abundant in the control group, significantly decreased in fatty liver conditions but was restored by TC + PL treatment, indicating a beneficial lipidomic effect.

In this study, we highlight the effectiveness of the TC + PL extract combination against HFD-induced changes in mice. We performed a detailed lipidomic analysis and identified specific lipid species that contribute to metabolic syndrome-related issues. Targeting these lipids could hold therapeutic potential. TC + PL at a human equivalent dose improved IR and reduced harmful lipids. Additionally, our research showcases the protective role of specific herbal extracts in a hepatic 3D spheroid model, while TC + PL effectively addressed metabolic disruptions in the HFD-fed mouse model of obesity. Further studies, including different models and dose-response investigations, can reinforce the benefits of TC + PL in mitigating obesity-related metabolic disorders and T2DM. This study underscores the potential of TC and PL combined to combat IR and hepatic lipid-related issues.

7. Conclusions

In this study, we demonstrate the protective effects of the TC + PL combination and Saroglitazar in mitigating HFD-induced metabolic changes in mice. TC + PL exhibits anti-inflammatory activity, enhances glucose tolerance and insulin sensitivity, and normalizes hepatic lipid profiles in HFD-fed mice. It also restores balance to various lipid categories and shows favorable effects on fibrosis and inflammatory genes in both the 3D spheroid model and HFD-fed mice. This suggests that TC + PL formulation may offer protection against metabolic abnormalities linked to T2DM and fatty liver and warrants clinical evaluation.

Data availability statement

The data that support the findings of this study are available from the corresponding author, upon reasonable request.

CRediT authorship contribution statement

Deepika Kumari: Data curation, Formal analysis, Methodology, Validation, Writing – original draft, Writing – review & editing. **Jyoti Gautam:** Data curation, Formal analysis, Investigation, Methodology, Writing – original draft, Writing – review & editing. **Vipin Sharma:** Formal analysis, Investigation, Methodology, Data curation, Validation, Visualization. **Sonu Gupta:** Data curation, Formal analysis, Investigation, Methodology, Validation, Visualization. **Soumalya Sarkar:** Formal analysis, Investigation, Methodology. **Pradipta Jana:** Data curation, Formal analysis, Investigation, Methodology, Validation, Visualization. **Vikas Singhal:** Formal analysis, Investigation. **Prabhakar Babele:** Formal analysis, Investigation, Data curation. **Parul Kamboj:** Data curation, Investigation, Methodology. **Sneh Bajpai:** Data curation, Formal analysis, Investigation, Methodology, Validation, Visualization, Writing – original draft, Writing – review & editing. **Ruchi Tandon:** Data curation, Formal analysis, Investigation, Methodology, Supervision, Validation, Visualization, Writing – original draft, Writing – review & editing. **Yashwant Kumar:** Data curation, Formal analysis, Investigation, Methodology, Software, Supervision, Validation, Visualization, Writing – original draft, Writing – review & editing. **Madhu Dikshit:** Conceptualization, Data curation, Formal analysis, Funding acquisition, Investigation, Methodology, Project administration, Resources, Supervision, Validation, Visualization, Writing – original draft, Writing – review & editing.

Declaration of competing interest

The authors declare that they have no known competing financial interests or personal relationships that could have appeared to influence the work reported in this paper.

Acknowledgements and Funding

The authors express their gratitude to the Ministry of AYUSH and Department of Biotechnology (DBT), Government of India, for joint funding to carry out the research work presented in this manuscript (Grant Nos.: BT/PR40738/TRM/120/486/2020 and A.11019/03/2020-NMPB-IV-A). Madhu Dikshit also acknowledges the financial support from JBR/2020/000034 and CCRAS (HQ-PROJ011/20/2022-PROJ). We acknowledge THSTI Small Animal Facility (SAF) for the services. We also appreciate the technical assistance provided by Mr. Sebanta Pokhrel, Miss. Siva Swapna Kasarla and Mr. Amit Kumar from THSTI during the study.

Appendix A. Supplementary data

Supplementary data to this article can be found online at https://doi.org/10.1016/j.heliyon.2023.e22051.

References

[1] M. Benedict, X. Zhang, Non-alcoholic fatty liver disease: an expanded review, World J. Hepatol. 9 (16) (2017) 715–732.
[2] H. Kolb, S. Martin, Environmental/lifestyle factors in the pathogenesis and prevention of type 2 diabetes, BMC Med. 15 (1) (2017) 131.
[3] S. Sarkar, et al., Hypoxia aggravates non-alcoholic fatty liver disease in presence of high fat choline deficient diet: a pilot study, Life Sci. 260 (2020), 118404.
[4] A.M. Gusdon, K.X. Song, S. Qu, Nonalcoholic Fatty liver disease: pathogenesis and therapeutics from a mitochondria-centric perspective, Oxid. Med. Cell. Longev. 2014 (2014), 637027.
[5] M. Shao, et al., Abnormal metabolic processes involved in the pathogenesis of non-alcoholic fatty liver disease (Review), Exp. Ther. Med. 20 (5) (2020), 26.
[6] E. Burgos-Moron, et al., Relationship between oxidative stress, ER stress, and inflammation in type 2 diabetes: the battle continues, J. Clin. Med. 8 (9) (2019).
[7] T. Yuan, et al., New insights into oxidative stress and inflammation during diabetes mellitus-accelerated atherosclerosis, Redox Biol. 20 (2019) 247–260.
[8] M. Modak, et al., Indian herbs and herbal drugs used for the treatment of diabetes, J. Clin. Biochem. Nutr. 40 (3) (2007) 163–173.
[9] H. Yao, et al., Herbal medicines and nonalcoholic fatty liver disease, World J. Gastroenterol. 22 (30) (2016) 6890–6905.
[10] Y. Xu, et al., Herbal medicine in the treatment of non-alcoholic fatty liver diseases-efficacy, action mechanism, and clinical application, Front. Pharmacol. 11 (2020) 601.
[11] T. Yan, et al., Herbal drug discovery for the treatment of nonalcoholic fatty liver disease, Acta Pharm. Sin. B 10 (1) (2020) 3–18.
[12] D.P. Singh, et al., Hepatoprotective effect of A polyherbal extract containing Andrographis paniculata, Tinospora cordifolia and Solanum nigrum against paracetamol induced hepatotoxicity, Phcog. Mag. 11 (Suppl 3) (2015) S375–S379.
[13] P.D. Nadig, et al., Effect of Tinospora cordifolia on experimental diabetic neuropathy, Indian J. Pharmacol. 44 (5) (2012) 580–583.

[14] V. Sharma, D. Pandey, Protective role of Tinospora cordifolia against lead-induced hepatotoxicity, Toxicol. Int. 17 (1) (2010) 12–17.
[15] H. Singh, et al., Tinospora cordifolia attenuates high fat diet-induced obesity and associated hepatic and renal dysfunctions in rats, PharmaNutrition 13 (2020), 100189.
[16] A.J. Christina, et al., Inhibition of CCl4-induced liver fibrosis by Piper longum Linn.? Phytomedicine 13 (3) (2006) 196–198.
[17] I.B. Koul, A. Kapil, Evaluation of the liver protective potential of piperine, an active principle of black and long peppers, Planta Med. 59 (5) (1993) 413–417.
[18] M.H. Abu Bakar, et al., Withaferin A protects against high-fat diet-induced obesity via attenuation of oxidative stress, inflammation, and insulin resistance, Appl. Biochem. Biotechnol. 188 (1) (2019) 241–259.
[19] D.P. Patel, et al., Withaferin A improves nonalcoholic steatohepatitis in mice, J. Pharmacol. Exp. Therapeut. 371 (2) (2019) 360–374.
[20] H.M.A. Khalil, et al., Ashwagandha (Withania somnifera) root extract attenuates hepatic and cognitive deficits in thioacetamide-induced rat model of hepatic encephalopathy via induction of Nrf2/HO-1 and mitigation of NF-kappaB/MAPK signaling pathways, J. Ethnopharmacol. 277 (2021), 114141.
[21] T. Anwer, et al., Effect of Withania somnifera on insulin sensitivity in non-insulin-dependent diabetes mellitus rats, Basic Clin. Pharmacol. Toxicol. 102 (6) (2008) 498–503.
[22] M. Alizadeh, et al., Changes of insulin resistance and adipokines following supplementation with Glycyrrhiza glabra L. Extract in combination with a low-calorie diet in overweight and obese subjects: a randomized double blind clinical trial, Adv. Pharmaceut. Bull. 8 (1) (2018) 123–130.
[23] S.K. Maurya, K. Raj, A.K. Srivastava, Antidyslipidaemic activity of Glycyrrhiza glabra in high fructose diet induced dsyslipidaemic Syrian golden hamsters, Indian J. Clin. Biochem. 24 (4) (2009) 404–409.
[24] C. Wang, et al., Protective effects of glycyrrhizic acid from edible botanical glycyrrhiza glabra against non-alcoholic steatohepatitis in mice, Food Funct. 7 (9) (2016) 3716–3723.
[25] T. Yan, et al., Glycyrrhizin alleviates nonalcoholic steatohepatitis via modulating bile acids and meta-inflammation, Drug Metab. Dispos. 46 (9) (2018) 1310–1319.
[26] L. Yang, et al., The anti-diabetic activity of licorice, a widely used Chinese herb, J. Ethnopharmacol. 263 (2020), 113216.
[27] M. Dushkin, et al., Effects of rhaponticum carthamoides versus glycyrrhiza glabra and punica granatum extracts on metabolic syndrome signs in rats, BMC Compl. Alternative Med. 14 (2014) 33.
[28] H.T. Chan, C. Chan, J.W. Ho, Inhibition of glycyrrhizic acid on aflatoxin B1-induced cytotoxicity in hepatoma cells, Toxicology 188 (2–3) (2003) 211–217.
[29] S. Kumar, et al., Picrorhiza kurroa enhances beta-cell mass proliferation and insulin secretion in streptozotocin evoked beta-cell damage in rats, Front. Pharmacol. 8 (2017) 537.
[30] S.N. Shetty, et al., A study of standardized extracts of Picrorhiza kurroa Royle ex Benth in experimental nonalcoholic fatty liver disease, J. Ayurveda Integr. Med. 1 (3) (2010) 203–210.
[31] S. Phoboo, et al., Phenolic-linked biochemical rationale for the anti-diabetic properties of Swertia chirayita (Roxb. ex Flem.) Karst, Phytother Res. 27 (2) (2013) 227–235.
[32] A. Saifudin, S. Kadota, Y. Tezuka, Protein tyrosine phosphatase 1B inhibitory activity of Indonesian herbal medicines and constituents of Cinnamomum burmannii and Zingiber aromaticum, J. Nat. Med. 67 (2) (2013) 264–270.
[33] M.S. Gundeti, et al., AYUSH 64, a polyherbal Ayurvedic formulation in Influenza-like illness - results of a pilot study, J. Ayurveda Integr. Med. 13 (1) (2022), 100325.
[34] A.K. Panda, et al., AYUSH- 64: a potential therapeutic agent in COVID-19, J. Ayurveda Integr. Med. 13 (2) (2022), 100538.
[35] H. Singh, et al., AYUSH-64 as an adjunct to standard care in mild to moderate COVID-19: an open-label randomized controlled trial in Chandigarh, India, Compl. Ther. Med. 66 (2022), 102814.
[36] R.G. Reddy, et al., AYUSH-64 as an add-on to standard care in asymptomatic and mild cases of COVID-19: a randomized controlled trial, Ayu 41 (2) (2020) 107–116.
[37] M.S. Winzell, B. Ahren, The high-fat diet-fed mouse: a model for studying mechanisms and treatment of impaired glucose tolerance and type 2 diabetes, Diabetes 53 (Suppl 3) (2004) S215–S219.
[38] C.Y. Wang, J.K. Liao, A mouse model of diet-induced obesity and insulin resistance, Methods Mol. Biol. 821 (2012) 421–433.
[39] J. Gautam, et al., Characterization of lipid signatures in the plasma and insulin-sensitive tissues of the C57BL/6J mice fed on obesogenic diets, Biochim. Biophys. Acta Mol. Cell Biol. Lipids 1868 (9) (2023), 159348.
[40] M. Alves-Bezerra, D.E. Cohen, Triglyceride metabolism in the liver, Compr. Physiol. 8 (1) (2017) 1–8.
[41] P. Nguyen, et al., Liver lipid metabolism, J. Anim. Physiol. Anim. Nutr. 92 (3) (2008) 272–283.
[42] N. Namazi, et al., The effect of dried Glycyrrhiza glabra L. Extract on obesity management with regard to PPAR-gamma2 (Pro12Ala) gene polymorphism in obese subjects following an energy restricted diet, Adv. Pharmaceut. Bull. 7 (2) (2017) 221–228.
[43] S. Gawrieh, et al., Saroglitazar, a PPAR-alpha/gamma agonist, for treatment of NAFLD: a randomized controlled double-blind phase 2 trial, Hepatology 74 (4) (2021) 1809–1824.
[44] D.P. Kumar, et al., The PPAR alpha/gamma agonist Saroglitazar improves insulin resistance and steatohepatitis in a diet induced animal model of nonalcoholic fatty liver disease, Sci. Rep. 10 (1) (2020) 9330.
[45] A. Sosale, B. Saboo, B. Sosale, Saroglitazar for the treatment of hypertrig-lyceridemia in patients with type 2 diabetes: current evidence, Diabetes Metab Syndr Obes 8 (2015) 189–196.
[46] S. Sarkar, et al., Saroglitazar and Hepano treatment offers protection against high fat high fructose diet induced obesity, insulin resistance and steatosis by modulating various class of hepatic and circulating lipids, Biomed. Pharmacother. 144 (2021), 112357.
[47] P. Pingitore, et al., Human multilineage 3D spheroids as a model of liver steatosis and fibrosis, Int. J. Mol. Sci. 20 (7) (2019).
[48] S. Strobel, et al., A 3D primary human cell-based in vitro model of non-alcoholic steatohepatitis for efficacy testing of clinical drug candidates, Sci. Rep. 11 (1) (2021), 22765.
[49] S.S. Kasarla, et al., In vitro effect of Withania somnifera, AYUSH-64, and remdesivir on the activity of CYP-450 enzymes: implications for possible herb-drug interactions in the management of COVID-19, Front. Pharmacol. 13 (2022), 973768.
[50] Z.A. Rizvi, et al., Pharmacological potential of Withania somnifera (L.) Dunal and Tinospora cordifolia (Willd.) Miers on the experimental models of COVID-19, T cell differentiation, and neutrophil functions, Front. Immunol. 14 (2023), 1138215.
[51] Z.A. Rizvi, et al., Prophylactic treatment of Glycyrrhiza glabra mitigates COVID-19 pathology through inhibition of pro-inflammatory cytokines in the hamster model and NETosis, Front. Immunol. 13 (2022), 945583.
[52] Z.A. Rizvi, et al., Effect of prophylactic use of intranasal Oil formulations in the hamster model of COVID-19, Front. Pharmacol. 12 (2021), 746729.
[53] Z.A. Rizvi, et al., Evaluation of ayush-64 (a polyherbal formulation) and its ingredients in the Syrian hamster model for SARS-CoV-2 infection reveals the preventative potential of Alstonia scholaris, Pharmaceuticals 16 (9) (2023).
[54] P.K. Sharma, et al., The aqueous root extract of Withania somnifera ameliorates LPS-induced inflammatory changes in the in vitro cell-based and mice models of inflammation, Front. Pharmacol. 14 (2023), 1139654.
[55] M.P.K. Dagar, M. Dikshit, A. Kumar, Pharmacological evaluations of select herbal extracts on TLR7/8-induced cytokine and chemokine production in macrophage-like cells, J Clin Exp Pharmacol 13 (2023) 374.
[56] D. Mundkinajeddu, et al., Development and validation of high performance liquid chromatography method for simultaneous estimation of flavonoid glycosides in Withania somnifera aerial parts, ISRN Analytical Chemistry 2014 (2014), 351547.
[57] V. Panda, et al., An Ayurvedic formulation of Emblica officinalis and Curcuma longa alleviates insulin resistance in diabetic rats: involvement of curcuminoids and polyphenolics, J. Ayurveda Integr. Med. 12 (3) (2021) 506–513.
[58] M. Schwaiger, et al., Merging metabolomics and lipidomics into one analytical run, a 144 (1) (2018) 220–229.
[59] J.P. Koelmel, et al., LipidMatch: an automated workflow for rule-based lipid identification using untargeted high-resolution tandem mass spectrometry data, BMC Bioinf. 18 (1) (2017) 331.

[60] M.R. Jain, et al., Dual PPARalpha/gamma agonist Saroglitazar improves liver histopathology and biochemistry in experimental NASH models, Liver Int. 38 (6) (2018) 1084–1094.
[61] R.E. Feaver, et al., Development of an in vitro human liver system for interrogating nonalcoholic steatohepatitis, JCI Insight 1 (20) (2016), e90954.
[62] S. Ahmad, et al., Indian medicinal plants and formulations and their potential against COVID-19-preclinical and clinical research, Front. Pharmacol. 11 (2020), 578970.
[63] M. Singh, et al., Withania somnifera (L.) Dunal (Ashwagandha) for the possible therapeutics and clinical management of SARS-CoV-2 infection: plant-based drug discovery and targeted therapy, Front. Cell. Infect. Microbiol. 12 (2022), 933824.
[64] S. Sen, et al., Diabetes mellitus and COVID-19: understanding the association in light of current evidence, World J Clin Cases 9 (28) (2021) 8327–8339.
[65] S.E. Shoelson, L. Herrero, A. Naaz, Obesity, inflammation, and insulin resistance, Gastroenterology 132 (6) (2007) 2169–2180.
[66] D. Kumar, et al., Saroglitazar reduces obesity and associated inflammatory consequences in murine adipose tissue, Eur. J. Pharmacol. 822 (2018) 32–42.
[67] K. Kesarwani, R. Gupta, A. Mukerjee, Bioavailability enhancers of herbal origin: an overview, Asian Pac. J. Trop. Biomed. 3 (4) (2013) 253–266.
[68] S. Kumar, et al., Overview for various aspects of the health benefits of Piper longum linn. fruit, J Acupunct Meridian Stud 4 (2) (2011) 134–140.
[69] V. Yadav, A. Krishnan, D. Vohora, A systematic review on Piper longum L.: bridging traditional knowledge and pharmacological evidence for future translational research, J. Ethnopharmacol. 247 (2020), 112255.
[70] G.B. Dudhatra, et al., A Comprehensive Review on Pharmacotherapeutics of Herbal Bioenhancers, ScientificWorldJournal 2012 (2012), 637953.
[71] A. Khajuria, et al., Piperine modulation of carcinogen induced oxidative stress in intestinal mucosa, Mol. Cell. Biochem. 189 (1–2) (1998) 113–118.
[72] K. Bechynska, et al., The effect of mycotoxins and silymarin on liver lipidome of mice with non-alcoholic fatty liver disease, Biomolecules 11 (11) (2021).
[73] A. Moomin, et al., Season, storage and extraction method impact on the phytochemical profile of Terminalia ivorensis, BMC Plant Biol. 23 (1) (2023) 162.
[74] B. Sultana, F. Anwar, M. Ashraf, Effect of extraction solvent/technique on the antioxidant activity of selected medicinal plant extracts, Molecules 14 (6) (2009) 2167–2180.
[75] C. Onyebuchi, D. Kavaz, Effect of extraction temperature and solvent type on the bioactive potential of Ocimum gratissimum L. extracts, Sci. Rep. 10 (1) (2020), 21760.
[76] V. Braunersreuther, et al., Role of cytokines and chemokines in non-alcoholic fatty liver disease, World J. Gastroenterol. 18 (8) (2012) 727–735.
[77] T.C.M. Fontes-Cal, et al., Crosstalk between plasma cytokines, inflammation, and liver damage as a New strategy to monitoring NAFLD progression, Front. Immunol. 12 (2021), 708959.
[78] S. Leon-Cabrera, et al., Reduced systemic levels of IL-10 are associated with the severity of obstructive sleep apnea and insulin resistance in morbidly obese humans, Mediators Inflamm 2015 (2015), 493409.
[79] T. Biedermann, M. Röcken, Pro- and anti-inflammatory effects of IL-4: from studies in mice to therapy of autoimmune diseases in humans, in: Animal Models of T Cell-Mediated Skin Diseases, Springer Berlin Heidelberg, Berlin, Heidelberg, 2005.
[80] G. Anovazzi, et al., Functionality and opposite roles of two interleukin 4 haplotypes in immune cells, Genes Immun 18 (1) (2017) 33–41.
[81] M.Y. Shiau, et al., Mechanism of interleukin-4 reducing lipid deposit by regulating hormone-sensitive lipase, Sci. Rep. 9 (1) (2019), 11974.
[82] R.L. Gieseck 3rd, M.S. Wilson, T.A. Wynn, Type 2 immunity in tissue repair and fibrosis, Nat. Rev. Immunol. 18 (1) (2018) 62–76.
[83] T. Huby, E.L. Gautier, Immune cell-mediated features of non-alcoholic steatohepatitis, Nat. Rev. Immunol. 22 (7) (2022) 429–443.
[84] J. Li, et al., Therapeutic mechanisms of herbal medicines against insulin resistance: a review, Front. Pharmacol. 10 (2019) 661.
[85] H. Kitade, et al., Nonalcoholic fatty liver disease and insulin resistance: New insights and potential New treatments, Nutrients 9 (4) (2017).
[86] D.P. Koonen, et al., Increased hepatic CD36 expression contributes to dyslipidemia associated with diet-induced obesity, Diabetes 56 (12) (2007) 2863–2871.
[87] C.G. Wilson, et al., Hepatocyte-specific disruption of CD36 attenuates fatty liver and improves insulin sensitivity in HFD-fed mice, Endocrinology 157 (2) (2016) 570–585.
[88] Y.K. Lee, et al., Hepatic lipid homeostasis by peroxisome proliferator-activated receptor gamma 2, Liver Res 2 (4) (2018) 209–215.
[89] Y. Wang, et al., PPARs as metabolic regulators in the liver: lessons from liver-specific PPAR-null mice, Int. J. Mol. Sci. 21 (6) (2020).
[90] K. Matsusue, et al., Liver-specific disruption of PPARgamma in leptin-deficient mice improves fatty liver but aggravates diabetic phenotypes, J. Clin. Invest. 111 (5) (2003) 737–747.
[91] B. Knebel, et al., Liver-specific expression of transcriptionally active SREBP-1c is associated with fatty liver and increased visceral fat mass, PLoS One 7 (2) (2012), e31812.
[92] S. Casas-Grajales, P. Muriel, Antioxidants in liver health, World J Gastrointest Pharmacol Ther 6 (3) (2015) 59–72.
[93] E. Fjaere, et al., Tissue inhibitor of matrix metalloproteinase-1 is required for high-fat diet-induced glucose intolerance and hepatic steatosis in mice, PLoS One 10 (7) (2015), e0132910.
[94] A. Naim, Q. Pan, M.S. Baig, Matrix metalloproteinases (MMPs) in liver diseases, J Clin Exp Hepatol 7 (4) (2017) 367–372.
[95] M. Giannandrea, W.C. Parks, Diverse functions of matrix metalloproteinases during fibrosis, Dis Model Mech 7 (2) (2014) 193–203.
[96] B.D. Radbill, et al., Loss of matrix metalloproteinase-2 amplifies murine toxin-induced liver fibrosis by upregulating collagen I expression, Dig. Dis. Sci. 56 (2) (2011) 406–416.
[97] D. Jahn, et al., Animal models of NAFLD from a hepatologist's point of view, Biochim. Biophys. Acta, Mol. Basis Dis. 1865 (5) (2019) 943–953.
[98] K. Saito, et al., Characterization of hepatic lipid profiles in a mouse model with nonalcoholic steatohepatitis and subsequent fibrosis, Sci. Rep. 5 (2015), 12466.
[99] S. Liangpunsakul, N. Chalasani, Lipid mediators of liver injury in nonalcoholic fatty liver disease, Am. J. Physiol. Gastrointest. Liver Physiol. 316 (1) (2019) G75–G81.
[100] N. Fujiwara, et al., CPT2 downregulation adapts HCC to lipid-rich environment and promotes carcinogenesis via acylcarnitine accumulation in obesity, Gut 67 (8) (2018) 1493–1504.
[101] D. Serra, et al., Mitochondrial fatty acid oxidation in obesity, Antioxid Redox Signal 19 (3) (2013) 269–284.
[102] V.T. Samuel, et al., Inhibition of protein kinase Cepsilon prevents hepatic insulin resistance in nonalcoholic fatty liver disease, J. Clin. Invest. 117 (3) (2007) 739–745.
[103] Y.K. Kaneko, T. Ishikawa, Diacylglycerol signaling pathway in pancreatic beta-cells: an essential role of diacylglycerol kinase in the regulation of insulin secretion, Biol. Pharm. Bull. 38 (5) (2015) 669–673.
[104] D.L. Gorden, et al., Increased diacylglycerols characterize hepatic lipid changes in progression of human nonalcoholic fatty liver disease; comparison to a murine model, PLoS One 6 (8) (2011), e22775.
[105] A. Kotronen, et al., Hepatic stearoyl-CoA desaturase (SCD)-1 activity and diacylglycerol but not ceramide concentrations are increased in the nonalcoholic human fatty liver, Diabetes 58 (1) (2009) 203–208.
[106] D.L. Gorden, et al., Biomarkers of NAFLD progression: a lipidomics approach to an epidemic, J. Lipid Res. 56 (3) (2015) 722–736.
[107] P.T. Hawkins, L.R. Stephens, PI3K signalling in inflammation, Biochim. Biophys. Acta Mol. Cell Biol. Lipids 1851 (6) (2015) 882–897.
[108] Y.H. Huang, et al., Lysophosphatidylcholine (LPC) induces proinflammatory cytokines by a platelet-activating factor (PAF) receptor-dependent mechanism, Clin. Exp. Immunol. 116 (2) (1999) 326–331.
[109] L.S. Huang, et al., Lysophosphatidylcholine containing docosahexaenoic acid at the sn-1 position is anti-inflammatory, Lipids 45 (3) (2010) 225–236.
[110] L. Zhou, et al., Serum metabolic profiling study of hepatocellular carcinoma infected with hepatitis B or hepatitis C virus by using liquid chromatography-mass spectrometry, J. Proteome Res. 11 (11) (2012) 5433–5442.